HHS Public Access

Author manuscript

Cell Rep. Author manuscript; available in PMC 2023 September 27.

Published in final edited form as:

Cell Rep. 2023 August 29; 42(8): 112935. doi:10.1016/j.celrep.2023.112935.

Angiotensin AT_{1A} receptor signal switching in Agouti-related peptide neurons mediates metabolic rate adaptation during obesity

Kirthikaa Balapattabi[1], **Yavuz Yavuz**[2,3,4], **Jingwei Jiang**[2], **Guorui Deng**[2], **Natalia M. Mathieu**[1], **McKenzie L. Ritter**[1], **Megan A. Opichka**[1], **John J. Reho**[1,5], **John D. McCorvy**[6,7,8], **Pablo Nakagawa**[1,7,9], **Lisa L. Morselli**[9,10], **Gary C. Mouradian Jr.**[1,7,9], **Deniz Atasoy**[2,3,4], **Huxing Cui**[2,3,4], **Matthew R. Hodges**[1,7], **Curt D. Sigmund**[1,7,9], **Justin L. Grobe**[1,5,7,9,11,12,*]

[1]Department of Physiology, Medical College of Wisconsin, Milwaukee, WI 53226, USA

[2]Department of Neuroscience and Pharmacology, University of Iowa Carver College of Medicine, Iowa City, IA 52242, USA

[3]Fraternal Order of Eagles Diabetes Research Center, University of Iowa Carver College of Medicine, Iowa City, IA 52242, USA

[4]Iowa Neuroscience Institute, University of Iowa Carver College of Medicine, Iowa City, IA 52242, USA

[5]Comprehensive Rodent Metabolic Phenotyping Core, Medical College of Wisconsin, Milwaukee, WI 53226, USA

[6]Department of Cell Biology, Neurobiology and Anatomy, Medical College of Wisconsin, Milwaukee, WI 53226, USA

[7]Neuroscience Research Center, Medical College of Wisconsin, Milwaukee, WI 53226, USA

[8]Cancer Center, Medical College of Wisconsin, Milwaukee, WI 53226, USA

[9]Cardiovascular Center, Medical College of Wisconsin, Milwaukee, WI 53226, USA

[10]Department of Medicine, Division of Endocrinology, Medical College of Wisconsin, Milwaukee, WI 53226, USA

[11]Department of Biomedical Engineering, Medical College of Wisconsin, Milwaukee, WI 53226, USA

[12]Lead contact

*Correspondence: jgrobe@mcw.edu.

AUTHOR CONTRIBUTIONS

K.B., D.A., H.C., L.L.M., C.D.S., and J.L.G. conceived experiments. K.B., Y.Y., J.J., G.D., N.M.M., M.L.R., M.A.O., J.J.R., D.A., H.C., and J.L.G. performed studies and collected data. J.D.M., P.N., L.L.M., G.C.M., D.A., H.C., M.R.H., C.D.S., and J.L.G. provided resources, supervision, methodologies, models, and funding acquisition.

DECLARATION OF INTERESTS

The authors declare no competing interests.

SUPPLEMENTAL INFORMATION

Supplemental information can be found online at https://doi.org/10.1016/j.celrep.2023.112935.

SUMMARY

Resting metabolic rate (RMR) adaptation occurs during obesity and is hypothesized to contribute to failed weight management. Angiotensin II (Ang-II) type 1 (AT_{1A}) receptors in Agouti-related peptide (AgRP) neurons contribute to the integrative control of RMR, and deletion of AT_{1A} from AgRP neurons causes RMR adaptation. Extracellular patch-clamp recordings identify distinct cellular responses of individual AgRP neurons from lean mice to Ang-II: no response, inhibition via AT_{1A} and Gαi, or stimulation via Ang-II type 2 (AT_2) receptors and Gαq. Following diet-induced obesity, a subset of Ang-II/AT_{1A}-inhibited AgRP neurons undergo a spontaneous G-protein "signal switch," whereby AT_{1A} stop inhibiting the cell via Gαi and instead begin stimulating the cell via Gαq. DREADD-mediated activation of Gαi, but not Gαq, in AT_{1A}-expressing AgRP cells stimulates RMR in lean and obese mice. Thus, loss of AT_{1A}-Gαi coupling within the AT_{1A}-expressing AgRP neuron subtype represents a molecular mechanism contributing to RMR adaptation.

In brief

Balapattabi et al. discovered that a specific subtype of Agouti-related peptide (AgRP) neuron in the hypothalamic arcuate nucleus is inhibited by the angiotensin II type 1 receptor (AT_1R). Obesity causes AT_1R within this AgRP subtype to switch from inhibitory Gαi to stimulatory Gαq signaling, resulting in dysfunctional control of resting metabolism.

Graphical Abstract

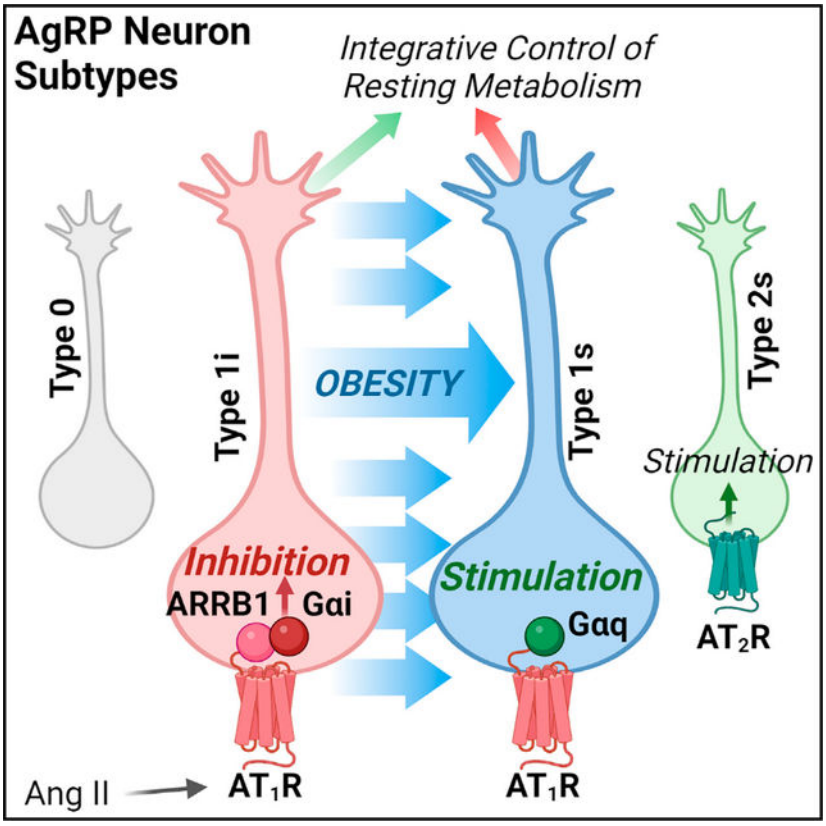

INTRODUCTION

Resting metabolic rate (RMR) normally accounts for approximately 70% of energy expenditure in humans.[1] Obesity is associated with "RMR adaptation," or the suppression of RMR relative to body size and composition,[2] and RMR adaptation has been proposed as a factor in weight regain after weight loss.[3] Thus, understanding the integrative control of RMR and the pathogenesis of RMR adaptation remains an important goal in the context of the ongoing obesity epidemic.

Circulating hormones including leptin and angiotensin II (Ang-II) contribute to RMR control, in part, by acting within the arcuate nucleus (ARC) of the hypothalamus to suppress inhibitory Agouti-related peptide (AgRP) neurotransmission.[4,5] Because the neural networks that control RMR are intricately intertwined with mechanisms controlling blood pressure (BP), many novel RMR-stimulating drugs inevitably cause hypertension and have been abandoned before reaching clinical use.[6] Thus, there is a critically unmet need to develop approaches to maintain or increase RMR without causing hypertension, which will depend on identifying unique molecular players differentiating mechanisms controlling RMR versus BP.[3,7,8]

We previously demonstrated that Ang-II type 1A (*Agtr1a*/AT_{1A}) receptors are expressed in a subset of AgRP neurons of the mouse ARC[5,9–11] and are required for integrative control of AgRP expression and RMR, independent of BP or feeding.[5,9,12] Further, using single-nucleus RNA sequencing, we recently demonstrated that obesity induced by prolonged high-fat diet (HFD) feeding results in changes in the transcriptomic signatures for leptin, CREB, and other relevant pathways in AgRP neurons.[13] These findings prompt the hypotheses that AT_{1A}-mediated control of AgRP neurotransmission contributes to the integrative control of RMR and that dysfunctions in this mechanism contribute to RMR adaptation. The goals of this study were thus (1) to understand normal AT_{1A} signaling within AgRP neurons in RMR control, (2) to clarify how AT_{1A} signaling in AgRP neurons is altered during obesity, and (3) to determine how dysfunctional AT_{1A} signaling within AgRP neurons mechanistically contributes to RMR adaptation during obesity.

RESULTS

AgRP neurons of lean mice exhibit heterogeneous responses to Ang-II

Loose-cell recordings of AgRP neurons in ARC of male and female Ai9^{Agrp} mice (tdTomato reporter is expressed in AgRP neurons) were performed to examine the effect of Ang-II on activity of AgRP neurons. Ang-II application resulted in one of three distinct electrical responses in individual AgRP neurons of both male and female lean mice (Figures 1A–1C). Approximately one-third of AgRP neurons did not respond to Ang-II, approximately one-third exhibited an Ang-II-induced decreased firing rate, and one-third exhibited an Ang-II-induced excitation.

This distribution of responses of AgRP neurons to Ang-II was confirmed in two additional independent animal models. First, loose-cell recordings were performed in *Npy-Gfp* mice (GFP reporter is expressed via the *Npy* promoter), as neuropeptide-Y (*Npy*) expression

is tightly colocalized with *Agrp* expression within the ARC. *Npy* neurons exhibited a distribution of electrical responses similar to that of Ang-II (Figures S1A–S1C). Second, calcium flux was assessed in AgRP neurons following microinjection of an adeno-associated virus (AAV) vector encoding Cre-dependent expression of GCaMP7 into the ARC of *Agrp*-Cre mice. Again, individual AgRP neurons exhibited an approximately equal distribution of no response, inhibition, or stimulation in response to Ang-II (Figures S1D and S1E).

Membrane potential and firing rate were also measured by whole-cell current-clamp recordings. Resting membrane potentials were similar across the three subtypes of AgRP neurons in both male and female $Ai9^{AgRP}$ mice. Ang-II caused membrane hyperpolarization in Ang-II-inhibited AgRP neurons and depolarized and markedly increased the firing rate of Ang-II-stimulated AgRP neurons, but had no effect on membrane potential of non-responsive neurons (Figures 1D and 1E). Finally, the time course for the Ang-II-mediated responses of inhibited and stimulated AgRP neurons was distinct. The maximal inhibition of spontaneous activity of inhibited AgRP neurons occurred at ~320 ± 50 s after Ang-II and was maintained throughout the duration of the protocol. In contrast, maximal excitation of stimulated AgRP neurons occurred within ~120 ± 20 s of Ang-II application ($p < 0.05$ versus inhibited). Collectively, these results identify three distinct subtypes of AgRP neurons in lean mice that can be functionally differentiated based on their responses to Ang-II.

In lean animals, Ang-II inhibits AgRP neurons via AT_1R and stimulates via AT_2R

We utilized both pharmacological and genetic approaches to identify the receptor dependence of Ang-II on each of the three AgRP neuron subtypes. First, we confirmed that repeated cycles of Ang-II application and washout did not cause tachyphylaxis (Figures S2A and S2B). Consequently, repeated cycles of Ang-II could be used to identify AgRP neuron subtypes before testing the effects of inhibitors. The AT_1R antagonist losartan abolished the Ang-II-induced decrease in firing rate in Ang-II-inhibited AgRP neurons in $Ai9^{AgRP}$ mice (Figures 2A–2C). Thus, subsequently we referred to the subset of AgRP neurons that were non-responsive to Ang-II as “type 0” and the subset that were inhibited via AT_1R as “Type 1i.” Losartan did not block the increased firing rate in the Ang-II-stimulated subset of AgRP neurons (Figures 2A–2C and S2C), suggesting the response was not mediated at AT_1R. Interestingly, the AT_2R antagonist PD-123319 abolished this effect (Figure 2D). Application of the AT_2R agonist, CGP-42112a, caused excitation in this subtype similar to that in Ang-II (Figure S2D). Thus, subsequently we referred to the subset of AgRP neurons that were stimulated via AT_2R as “Type 2s.” These results support a role for AT_1R in Type 1i responses to Ang-II, and a role for AT_2R in Type 2s responses to Ang-II.

Next, we employed multiple approaches to delineate the involvement of the two pharmacologically indistinguishable AT_1R subtypes present in the mouse genome (AT_{1A}/*Agtr1a*, versus AT_{1B}/*Agtr1b*). First, extracellular recording was performed in mice with genetic deletion of *Agtr1a* from AgRP neurons ($AT_{1A}^{AgRP\text{-}KO}$ mice).[9] Ang-II elicited only two types of electrical response in this animal model: an increased firing rate in one subset of AgRP neurons (i.e., the Type 2s response), and no response (Type 0) in the other subset, consistent with the complete loss of the Type 1i response (Figure 2E). Second, loose-cell recording was performed on labeled cells within the ARC of mice expressing the tdTomato

reporter in cells that express *Agtr1a* (Ai9^{AT1A}, generated by breeding the Ai9 reporter strain with mice expressing Cre-recombinase via the *Agtr1a* promoter in a P1 artificial chromosome transgene, termed BAC-AT1A-Cre[14]). Of these cells, 92% were inhibited by Ang-II application and 8% did not respond to Ang-II (Figure 2F). These findings, along with previous efforts utilizing *in situ* hybridization, reporter transgene expression, and single-cell RNA sequencing analyses, support the concept that within the ARC *Agtr1a* is expressed only in a subset of AgRP neurons, while *Agtr1b* expression is below detection limits in AgRP neurons.[5,9,10] Collectively these results demonstrate that the inhibitory effect of Ang-II upon Type 1i neurons is mediated through the AT_{1A} receptor and support *Agtr1a* as a marker of this unique neuronal subtype within the ARC.

In Type 1i AgRP neurons, the AT_{1A} receptor signals via the Gαi cascade to cause cellular inhibition

Second-messenger coupling of AT_{1A} in Type 1i AgRP neurons was assessed using slice preparations from Ai9^{AT1A} mice. Whereas pretreatment with the Gαi inhibitor pertussis toxin (PTX) abolished the inhibitory effect of Ang-II in Type 1i neurons, pretreatment with the Gαq inhibitor BIM-46187 had no effect (Figures 3A–3C). Importantly, the efficacy of BIM-46187 to attenuate Gαq signaling within AgRP neurons was confirmed in mice that express the Gαq-coupled hM3Dq designer receptors exclusively activated by designer drugs (DREADD) in these cells (hM3Dq^{AgRP} mice), as clozapine *N*-oxide (CNO)-induced activation of hM3Dq and electrical activity were attenuated by BIM-46187 (Figure S3A). Complementing this approach, the efficacy of Gαi activation within Type 1i AgRP neurons to cause cellular inhibition was also examined using the Gαi-coupled hM4Di DREADD. Loose-cell recordings of Type 1i AgRP neurons (i.e., inhibited by Ang-II) of mice expressing hM4Di in AgRP neurons (hM4Di^{AgRP} mice) demonstrated that CNO application decreased spontaneous activity (Figure 3D).

A panel of candidate ion channels hypothesized to mediate Ang-II-induced inhibition of Type 1i neurons was examined using pharmacological inhibitors. Loose-cell recordings were performed in slice preparations from Ai9^{AgRP} mice in the presence of artificial cerebrospinal fluid (aCSF) and Ang-II to identify Type 1i AgRP neurons, followed by a wash and incubation with the specific modulator before a second application of Ang-II. Whereas incubation with aCSF vehicle had no effect in blocking the inhibitory effect of Ang-II, incubation with tertiapin-Q (inhibitor of G-protein-coupled inwardly rectifying potassium [Kir3/GIRK] channels), FPL-64776 (voltage-gated calcium-channel agonist), or 4-aminopyridine (voltage-gated potassium-channel inhibitor) all significantly attenuated the effect of Ang-II in the Type 1i neuron (Figures 3E and S3B). In contrast, penitrem A (calcium-activated potassium-channel subunit alpha-1 [BK] channel inhibitor), CLP-257 (potassium chloride transporter member 5 [KCC2] agonist), and bumetanide (Na-K-Cl cotransporter-1 [NKCC1] inhibitor) each had little or no effect. We conclude that within the Type 1i AgRP neuron under normal physiological conditions, AT_{1A} signals via a Gαi-coupled second-messenger cascade to activate voltage-gated potassium efflux and inhibit voltage-gated calcium influx, ultimately to inhibit the activity of the cell.

Type 1i ARC AgRP neurons project to a subset of regions that receive ARC AgRP inputs

ARC AgRP neurons are known to project to a relatively wide array of brain regions.[15] To clarify the target regions of Type 1i AgRP neurons, we performed unilateral microinjection of an AAV encoding a Cre-recombinase- and flippase-dependent eYFP fluorescent reporter into the ARC of mice expressing Cre-recombinase via the *Agtr1a* promoter and flippase via the *Npy* promoter (Figure 4A).[16] eYFP fluorescence exhibited unilateral expression across the rostral-caudal ARC (Figures 4B and 4C). Subsequent evaluation of the distribution of eYFP fibers identified a restricted pattern, largely limited to the medial preoptic nucleus (MPO), supraoptic nucleus (SON), paraventricular nucleus (PVN), and bed nucleus of the stria terminalis (BNST) (Figures 4D–4I). Sparse innervation was noted in the dorsomedial hypothalamus, lateral hypothalamic area, amygdala, paraventricular nucleus of the thalamus, periaqueductal gray, and parabrachial nucleus (Figure S4). It is important to consider, however, that because of the intersectional genetic approach used here, the low number of axons labeled by the eYFP reporter may result in false-negative conclusions regarding projections of these neurons. Previously reported AgRP projections are illustrated in the upper panel of Figure 4J,[17,18] while qualitative visual estimation of relative eYFP fiber density across different brain regions is illustrated in the lower panel.

High-fat-diet-induced obesity induces a G-protein “signal switch” in some Type 1i AgRP neurons

Aga in, using loose-cell recordings, the electrical responses of AgRP neurons to Ang-II were examined after 10 weeks of exposure to HFD (45% kcal from fat). Surprisingly, after HFD (Figure 5A) a larger proportion of AgRP neurons exhibited stimulatory responses to Ang-II compared to chow-fed mice (previously shown as Figure 1C; χ^2 comparison of distributions, $p = 0.03$), although this deviation was only observed in male mice. To further understand the molecular basis of this change in male mice after HFD feeding, the receptor dependencies of responses to Ang-II were examined.

As before, individual AgRP neurons were not responsive to Ang-II (Type 0), inhibited through an AT_1R-mediated mechanism (Type 1i), or stimulated through an AT_2R-mediated mechanism (Type 2s). Interestingly, a new subtype of AgRP neuron also emerged after HFD feeding, which was stimulated by Ang-II through a losartan-dependent (i.e., AT_1R-mediated) mechanism (Figures 5B and 5C). Importantly, the Ang-II response was not sensitive to inhibition by PD-123319, indicating that AT_2R do not contribute to this stimulatory effect (Figure 5D). Thus, because these cells are stimulated via an AT_1R-dependent mechanism, we referred to this HFD-induced AgRP neuron subtype as “Type 1s.”

In both lean and HFD-fed mice, type 0 and type 2s subtypes of AgRP neurons each accounted for approximately one-third of the AgRP neuron population (Figures 5E and 5F). Type 1i AgRP neurons also accounted for approximately one-third of AgRP neurons in lean mice. The emergence of the new Type 1s subtype resulted in a redistribution of this fraction of the cells; however, Type 1i only accounted for 19% of AgRP neurons after HFD, and Type 1s accounted for 17%. These results prompt the concept that HFD feeding induces a “signal switch” within Type 1 AgRP neurons. After HFD, AT_1R signaling begins to promote

cellular stimulation (i.e., Type 1s response) instead of inhibition within individual Type 1 neurons.

Ten weeks of HFD feeding did not alter the Ang-II-mediated electrical responses of AgRP neurons in female mice. The relative proportion of Ang-II-unresponsive, -inhibited, and -stimulated subtypes of AgRP neurons remained the same in lean versus HFD-fed female mice (Figure S5A). While losartan abolished inhibitory responses to Ang-II, it had no effect on stimulatory responses after HFD (Figures S5B–S5D). This indicates that all Ang-II-stimulated cells in females were Type 2s and, further, that 10 weeks of HFD feeding failed to induce the subtype switch from Type 1i to Type 1s in females. This finding parallels observations by our group and others that female C57BL/6J mice are largely resistant to weight gain and cardiometabolic alterations as induced by 10 weeks of HFD.[19]

As in lean male mice, Type 1i cells from HFD-fed mice responded to Ang-II with an inhibitory response that was mediated through a losartan-dependent (AT_1R) and PTX-dependent (Gαi) mechanism, while blockade of Gαq via BIM-46187 had no modulatory effect (Figure 5G). In contrast, Type 1s cells from HFD-fed mice responded to Ang-II with a stimulatory response that was mediated through a losartan-dependent (AT_1R) and BIM-46187-dependent (Gαq) mechanism, while PTX had no effect(Figure 5H). Collectively, these data demonstrate that 10 weeks of HFD feeding—which is sufficient to disrupt normal integrative control of thermogenesis and energy balance[19–21] and to robustly alter the transcriptome of AgRP neurons within the ARC[13] in male C57BL/6J mice—is associated with a spontaneous G-protein “signal switch” by the AT_1R within a subset of AgRP neurons, which results in complete reversal of cellular responses to AT_1R activation.

Activation of Gαi within Type 1 AgRP neurons stimulates resting metabolism, while activation of Gαq has no major effect

To probe the physiological and pathophysiological significance of Gαi versus Gαq signaling within the Type 1 AgRP neuron in the control of metabolism, we used site-specific delivery of an AAV vector encoding Cre-dependent expression of DREADD into the ARC of both male and female BAC-AT1A-Cre mice to direct expression of hM4Di or hM3Dq, respectively, into Type 1 AgRP neurons. After 2 weeks of recovery, extracellular patch-clamp recordings were performed on these neurons to investigate the efficacy and specificity of the expressed DREADD. Ang-II caused cellular inhibition, confirming Type 1i identity (Figures 6A and 6B). CNO was applied to induce chemogenetic modulation of the DREADD-expressing cells, and 13 out of 15 identified hM4Di-expressing Type 1i AgRP neurons responded to CNO with a significant reduction in firing rate. Pretreatment with PTX blocked this CNO-induced suppression. In contrast, activation of hM3Dq by CNO resulted in the robust activation of firing rate in 14 out of 17 cells, and BIM-46187 significantly attenuated this effect (Figures 6A and 6C). CNO did not influence the spontaneous activity of either hM4Di- or hM3Dq-deficient cells (Figures S6A and S6B).

A separate cohort of BAC-AT1A-Cre mice was maintained on chow diet or switched to HFD for 10 weeks (i.e., between 8 and 18 weeks of age). DREADD viruses were injected into the ARC at 16 weeks of age and metabolic responses to CNO injection were tested 2 weeks later. As expected, male but not female mice exhibited increased fat mass with HFD

feeding, and this effect was not modified by expression of either DREADD within type 1 AgRP neurons (Figures 6D and 6E). In parallel, only male mice exhibited a suppression of RMR after HFD feeding, and expression of the DREADD receptors did not modify this effect (Figure 6F). These results support two conclusions. First, HFD-induced RMR dysfunctions and AT_1R signal switching within Type 1 AgRP neurons both correlate with changes in body composition and not simply with HFD feeding. Second, because females did not exhibit changes in RMR control, body composition, or signal switching in response to HFD feeding, this suggests that the correlations among these effects may occur if females were exposed to a more robust obesogenic stimulus.

Finally, these mice were tested for acute RMR responses to activation of the DREADD receptors within Type 1 neurons. Injection of CNO had no effect on RMR in control mice and no major effect on RMR in mice expressing the Gαq-coupled hM3Dq receptor (Figure 6G). In contrast, CNO significantly increased RMR in both male and female mice expressing the Gαi-coupled hM4Di receptor, regardless of diet. Because no significant modulatory effect of sex was observed, reanalysis of the dataset with sexes combined clearly illustrate that activation of hM4Di similarly stimulates RMR in mice fed chow or HFD, while activation of hM3Dq had no significant effect on RMR regardless of diet (Figure 6H). These findings indicate that activation of Gαi signaling within type 1 AgRP neurons is sufficient to stimulate RMR even after prolonged HFD feeding. By extension, obesity-associated dysfunctions in RMR control appear to be secondary to the loss of AT_1R-Gαi coupling in these cells rather than the gain of AT_1R-Gαq coupling.

Previous work by various other groups has demonstrated that DREADD-mediated activation of Gαq or Gαi signaling within AgRP neurons has robust effects on feeding behavior.[22] Surprisingly, activation of Gαi or Gαq only within the Type 1 subtype of AgRP neurons had no effect on food intake in chow-fed or HFD-fed mice (Figures S6C–S6E). These findings imply that other subtypes (Types 0 and 2) of AgRP neuron contribute to the control of feeding behaviors.

Potential role for β-arrestin-1 in mediating AT_{1A}-Gαi coupling in Type 1 AgRP neurons

Coupling of G-protein-coupled receptors (GPCRs) to second-messenger cascades is mediated through a combination of receptor conformation, modifications, or decorations of the receptor, interactions with enzymes such as GPCR kinases, and interactions with β-arrestins.[23–28] Thus, it follows that HFD-induced “signal switching” within the AgRP neuron may be mediated through altered interactions between the AT_1R and these modulators of second-messenger cascade engagement.

One previous study demonstrated that mice harboring null alleles for β-arrestin-1 (*Arrb1*; *Arrb1*^{NULL} mice) are sensitized to HFD-induced weight gain due to suppressed energy expenditure, while mice with global transgenic (over)expression of *Arrb1* exhibit increased energy expenditure and are protected against HFD-induced weight gain and adiposity.[29] Another more recent study identified a role for β-arrestin-1 specifically within AgRP neurons in energy balance and glycemic control.[30] The team determined that within *Agrp*-expressing cells β-ar restin-1, but not β-arrestin-2 (*Arrb2*), is critically involved in electrochemical and physiological responses to insulin and obesogenic stimuli. For example,

Arrb1 overexpression in AgRP neurons resulted in a significant reduction in fat mass despite no changes in food-intake behaviors, implying increased energy expenditure.[30] We therefore probed the hypothesis that a β-arrestin-mediated pathway is involved in AT_1R signaling within Type 1i AgRP neurons. First, we examined electrophysiological responses of Type 1i neurons isolated from lean $Ai9^{AgRP}$ mice to the β-arrestin-biased AT_1R agonist, TRV120027 (TRV027). Identity of the cell as a Type 1i neuron was confirmed first by inhibitory responses to Ang-II. Subsequent application of TRV027 caused inhibition of the cell, and this effect was not additive to subsequent addition of Ang-II (Figure 7A). In contrast, preincubation of the cells with losartan or PTX each ameliorated the inhibitory response to TRV027 (Figure 7B). Previous work using bioluminescence resonance energy transfer proximity analyses in HEK293 cells suggested that TRV027, although touted as a biased agonist at the AT_1R to stimulate β-arrestin and not Gαq signaling, may also act as a partial agonist with low to moderate efficacy to stimulate Gαi2, Gαi3, and Gα12 signaling.[31] Therefore, the effect of TRV027 in inhibiting the Type 1 AgRP neuron is mediated by a PTX-sensitive Gαi cascade, but the involvement of β-arrestins in this mechanism remains unclear.

Thus, we next generated two mouse models with conditional deletion of either *Arrb1* (*Arrb1*$^{Agrp\text{-KO}}$ mice) or *Arrb2* (*Arrb2*$^{Agrp\text{-KO}}$ mice) from AgRP neurons and evaluated the distribution of cells that were stimulated, inhibited, or non-responsive to Ang-II. Compared to the relatively even distribution of responses by individual AgRP neurons in the ARC of lean $Ai9^{AgRP}$ mice (Figure 1C), AgRP cells that exhibited inhibitory responses to Ang-II were under-represented in the ARC of *Arrb1*$^{Agrp\text{-KO}}$ mice (sexes combined χ^2, $p < 0.01$; comparing sexes within *Arrb1*$^{Agrp\text{-KO}}$ group, $p = 0.87$) (Figure 7C). Responses of AgRP neurons from *Arrb2*$^{Agrp\text{-KO}}$ mice, in contrast, were distributed similarly to those of $Ai9^{AgRP}$ mice (sexes combined χ^2, $p = 0.95$; comparing sexes within *Arrb2*$^{Agrp\text{-KO}}$ group, $p = 0.90$) (Figure 7D).

Together, these data support the general concept that under normal physiological conditions, the AT_1R in Type 1 AgRP neurons couples through a signaling cascade that involves both β-arrestin-1 and Gαi (Figure 7E), but perhaps not β-arrestin-2. This mechanism becomes uncoupled during prolonged obesity, resulting in loss of inhibitory responses to AT_1R signaling and, ultimately, dysfunctional integrative control of resting metabolism. Because female *Arrb1*$^{Agrp\text{-KO}}$ mice appear to exhibit a loss of Ang-II-inhibited AgRP neurons similar to that of males, this may also hint that females exhibit resistance to diet-induced signal switching due to sex-dependent differences in molecular mechanisms regulating ARRB1 and/or Gαi recruitment to AT_1R in Type 1 AgRP neurons.

DISCUSSION

Previous studies have implicated AgRP neurons in the integrative control of energy balance, and increasing evidence supports the existence of multiple subtypes of AgRP neurons.[5,9,11,32,33] Here we document three subtypes that can be dissociated based on their electrochemical responses to Ang-II. Further, we document the receptor dependencies and associated second-messenger cascades that mediate these responses, with one subtype (Type 1) exhibiting an inhibitory response via AT_1R, and one subtype (Type 2) exhibiting

a stimulatory response via AT_2R. Under normal physiological conditions the signal transduction of AT_1R within Type 1 neurons is mediated via a Gαi-coupled cascade that contrasts AT_1R transduction mechanisms in other neurons and other cell types throughout the body. The Type 1 subtype also only projects to a subset of the second-order brain regions that are known to receive ARC AgRP neuron projections. Most interestingly, we determined that prolonged HFD feeding results in a spontaneous G-protein "signal switch" by the AT_1R receptor within the Type 1 AgRP neuron subtype, from a Gαi-coupled cascade to a Gαq-coupled cascade, resulting in a complete reversal of the electrochemical responses of this neuron to Ang-II. As we have previously implicated AT_1R signaling within AgRP neurons in the integrative control of RMR,[5,9] this HFD-induced signal switch within the Type 1 subtype likely represents a molecular basis of obesity-associated dysfunctional control of RMR. Finally, DREADD-mediated stimulation of Gαi signaling in Type 1 AgRP neurons is sufficient to stimulate RMR even after HFD feeding while stimulation of Gαq signaling had no effect, indicating that the signal transduc- tion mechanisms responding to Gαi signaling within the Type 1 neuron remain largely intact during obesity. Further, these findings suggest that resulting dysfunctional control of RMR is the result of the loss of AT_1R-Gαi coupling in Type 1 neurons rather than the gain of AT_1R-Gαq coupling.

It is known that AT_1R can couple to various G-protein cascades and β-arrestin pathways, and clarifying the mechanisms that dictate biased signaling through any individual pathway represents a major ongoing effort by multiple groups. Early work identified the third intracellular loop of AT_1R as critical to mediating its interactions with G proteins,[34] and more recent work has provided much more detailed identification of specific intracellular domains that mediate interactions with various G proteins and β-arrestin partners.[26,31] Biased ligands for AT_1R are understood to differentially activate specific second-messenger cascades, and this is thought to occur through the induction of unique conformations of AT_1R, GPCR kinase (GRK)-mediated phosphorylation of different combinations of residues in the intracellular domains, or orthosteric or allosteric modulation of the intracellular conformational states of the receptor.[31,35–41] While AT_1R signaling through Gαq is thought to represent the dominant mode of signal transduction by this receptor in most tissues and has been disproportionately studied in various tissue types *in vivo* and *in vitro*, AT_1R has been documented to couple to the PTX-sensitive Gαi cascade in multiple tissues including rat adrenal glomerulosa, liver, kidney, and pituitary glands.[31,42–44] The present work, in contrast, documents a spontaneous change in the signaling cascade activated by AT_1R within a single *in vivo* cell type in response to its endogenous Ang-II ligand and the association of such a change with a pathophysiological outcome. This finding underscores the critical need to clarify the context dependency (cell type, disease state) of AT_1R coupling to various cascades. Further, this finding prompts a reconsideration of the potential context dependency of AT_1R signaling modalities in response to other synthetic and biased ligands. For example, while much of the work mapping second-messenger signaling in response to Ang-II and other ligands is performed in immortalized cells or tissues from healthy lean animals, re-evaluation of cell-type-specific signaling during pathological states such as hypertension, heart failure, obesity, and diabetes may uncover unexpected signaling events and identify novel therapeutic targets.

The general concept that electrochemical responses to neuronal AT_1R activation may be altered during HFD feeding has been hinted at previously. For example, de Kloet et al. previously demonstrated that few or no neurons of the PVN are inhibited by Ang-II,[45] which suggests that the normal signaling mechanism of AT_1R within PVN neurons is distinct from the Gαi-coupled pathway employed by Type 1i AgRP neurons within the arcuate. Interestingly, however, they determined that HFD feeding increased the proportion of PVN parvocellular neurons that were stimulated by Ang-II. This may reflect an increase in AT_1R expression or cell-surface localization, increased coupling efficiency to Gαq, or changes in signal termination, which may each involve molecular mechanisms that are shared by Type 1 AgRP neurons. Similar to their conclusions, the data presented herein support the concept that weight/adiposity gains, rather than diet composition, likely represents the driver of signal switching within Type 1 AgRP neurons.

Several possible molecular mechanisms that underlie the observed change in second-messenger signaling by AT_1R must be investigated. Our primary working hypothesis is focused on changes in the intracellular modulators of second-messenger coupling efficiency. Data presented in Figure 7 hint that conditional deletion of *Arrb1* within AgRP neurons is sufficient to cause redistribution of responses to Ang-II that parallel effects of prolonged HFD. Previous work by Pydi et al. implicated *Arrb1* within AgRP neurons in modulation of glycemic control and energy balance,[30] although the specific roles for *Arrb1* within subtypes of AgRP neuron remain unresolved. The “phosphorylation barcoding” hypothesis has been forwarded by multiple groups as a model to explain how intracellular regulators such as GRKs can differentially decorate the intracellular portions of a GPCR and thereby modify the relative affinity of that GPCR to recruit binding partners such as G proteins and β-arrestins.[23,27,46,47] We therefore hypothesize that obesity modifies the abundance or action of modulators such as GRKs within the Type 1 AgRP neuron, thereby altering phosphorylation patterns of AT_1R and the relative affinity of AT_1R for the Gαi versus Gαq cascades. Whether obesity induces signal switching in other cell types, whether signal switching affects other receptor types in AgRP and other cell types, and the mechanism by which obesity induces signal switching all represent critical future directions of inquiry.

Another hypothesized mechanism that may contribute to signal switching involves changes in the relative abundance of second-messenger cascade components. For example, the Kapusta and Wainford groups have demonstrated that under various conditions, the levels of individual G proteins can be altered within regions of the hypothalamus and that experimental depletion of individual G proteins can cause phenotypic changes *in vivo*.[48–51] Thus, it follows that the availability of Gαi proteins (in addition to, or instead of, altered affinity of AT_1R for Gαi) might become reduced in Type 1 neurons during HFD feeding. Ultimately, this would result in increased association of AT_1R with other binding partners, subject to both their relative affinities and abundances within the cell.

Many additional hypotheses might also be considered. For example, if obesity changes local levels of the Ang-II ligand within the interstitial space versus the synaptic clefts in the ARC or if the cellular localization of AT_1R changes during obesity (e.g., redistributes among the synaptic cleft versus the rest of the cell surface), the function of AT_1R might be expected to change. Homodimerization of AT_1R or its heterodimerization with other

receptors might alter the receptor's signaling kinetics,[52] and it is possible that obesity modulates these processes. Stretch of the cell membrane has been implicated as a ligand-independent modulator of AT_1R signaling,[53] and it follows that changes in os motic stresses upon the AgRP neuron during obesity may influence AT_1R signaling. Spontaneous ligand-independent activity of AT_1R in the absence of Ang-II is estimated to occur in ≈5% of these receptors in any given cell,[54] and if obesity alters that rate or the total abundance of receptors in the cell, this may also influence AT_1R signaling. All of these mechanisms may therefore independently or synergistically contribute to obesity-associated signal switching in the Type 1 AgRP neuron.

Instead of a signal switch from AT_1R coupling to Gαi to Gαq within an individual Type 1 AgRP neuron after prolonged HFD feeding, yet another potential explanation for the observed redistribution of AgRP neuron subtypes could involve recruitment of other neuron types into the pool of *Agrp*-expressing neurons. It is conceivable that HFD feeding causes other neuron types within the ARC to begin expressing both *Agrp* and *Agtr1a*. If such cells would normally exhibit AT_1R-Gαq coupling, this might also help explain the current observations by diluting the total pool of AgRP neurons. Alternatively, it is conceivable that Type 0 or Type 2 AgRP neurons might start expressing AT_1R. Such scenarios seem unlikely, however, because the relative proportions of Type 0 and Type 2s AgRP neurons were not altered by HFD feeding. Additional studies of the transcriptomes of individual AgRP neuron types after HFD feeding are required to address these ideas, but current single-cell/single-nucleus RNA sequencing methods provide insufficient sequencing depth to consistently resolve expression levels of GPCRs including AT_1R in individual neuron subtypes. Approaches such as Patch-to-Seq may prove beneficial in this regard.[55]

Despite the canonical role of AgRP neurons in the control of feeding behavior,[56] the Type 1 AgRP subtype appears to specifically contribute to the control of energy expenditure but not food intake. Deletion of the leptin receptor (*Lepr*) from AgRP neurons results in accelerated body mass and adipose gains despite normal food intake, implying a reduction in energy expenditure.[57] We previously demonstrated that deletion of AT_{1A} receptors (*Agtr1a*) from *Lepr*-expressing cells results in major disruption in the integrative control of energy expenditure without any notable effect on food intake.[9] In addition, although transgenic activation of the brain renin-angiotensin system (RAS), induction of the endogenous brain RAS through deoxycorticosterone acetate (DOCA)-salt treatment, or infusion of exogenous Ang-II into the brain have variable effects upon feeding behaviors, each of these manipulations strongly induces energy expenditure through the AT_1R.[9,58–61] Critically, the stimulation of energy expenditure by DOCA-salt treatment or exogenous Ang-II application to the brain is dependent upon the melanocortin type 4 receptor (MC_4R).[62] Because AgRP is an inverse agonist at the MC_4R, these findings support a working model in which various stimuli (e.g., leptin, DOCA-salt, Ang-II) all depend upon the activation of AT_1R on Type 1 AgRP neurons to suppress inhibitory AgRP neurotransmission to MC_4R on postsynaptic cells, presumably to disinhibit the activity of those target cells and ultimately stimulate resting metabolism.

The identity of relevant MC_4R-expressing second-order neurons represents a major focus for future study, but we hypothesize a role for projections to the preoptic area. Here

we determined that Type 1 AgRP neurons clearly extend to a subset of regions that receive projections from ARC AgRP neurons, including the PVN, MPO, BNST, and SON. Previous work investigating the consequences of manipulating MC_4R in cells that express *Sim1* (such as neurons of the PVN) demonstrate that MC_4R within the PVN is critically involved in the control of feeding but not energy expenditure.[63] While the SON is strongly implicated in the control of fluid and electrolyte homeostasis and MC_4R are known to be expressed in neurons in this region, the SON is not appreciated for a major role in energy balance.[64] A recent study using single-cell RNA sequencing and spatial mapping techniques to understand the cellular architecture of the preoptic area (including the MPO and BNST) demonstrated that MC_4R is expressed in a small number of glutamatergic neuron subtypes within the MPO but not the BNST.[65] In addition, microinjection of the melanocortin receptor agonist melanotan-II into the MPO of rats elicits thermogenic responses that are abolished by lesion of the dorsomedial hypothalamus.[66] As recently reviewed by Nakamura et al.,[67] the preoptic area including the MPO serves as a primary site of integrative control of thermoregulatory responses to various environmental stimuli. Although the neurocircuitry within the preoptic area governing responses to excess heat are generally mapped and typically involve inhibitory GABAergic neurons, the circuits and neuron types controlling responses to cold are less well clarified. These insights collectively lead us to a working model in which Type 1 AgRP neurons from the ARC project to the MPO to modulate activity of glutamatergic cold-sensitive neurons that express MC_4R and project to the dorsomedial hypothalamus to participate in the coordinated control of thermogenic autonomic activity. The activation of AT_1R on these Type 1 neurons therefore normally reduces inhibitory AgRP neurotransmission in this circuit, resulting in disinhibition of glutamatergic MC_4R-expressing target cells and, ultimately, the stimulation of thermogenesis. We posit that obesity-induced G-protein signal switching within the Type 1 neuron therefore causes adaptation of metabolic control through increased inhibitory AgRP neurotransmission.

Limitations of the study

Several limitations of the current study should be considered. First, we focused on the functions of AT_1R within Type 1 AgRP neurons but have not yet characterized the role(s) of Type 0 cells, or AT_2R within Type 2 AgRP neurons, in energy balance physiology. As our manipulations of Type 1 cell activity had no effect on feeding behavior, we conclude that the major effect of AgRP neurons upon feeding behavior are likely mediated through some combination of Type 0 and Type 2 subtypes. Second, we have not yet explored the possibility that G-protein signal switching induced by HFD feeding may occur at other receptors within the Type 1 AgRP neuron or in any other cell types. For example, ghrelin acts at AgRP neurons via its GPCR (*Ghsr*) to stimulate cell activity,[68] while glucagon-like peptide 1 acts via its GPCR (*Glp1r*) at AgRP neurons to inhibit cell activity.[69] Determining whether such receptors also undergo G-protein signal switching during pathological states such as obesity remains un-tested. Third, 10 weeks of HFD feeding was insufficient to induce a G-protein signal switch in Type 1 neurons from female mice. This observation correlates well with the resistance of female C57BL/6J mice to gain excessive weight with HFD feeding. Preliminary studies of females fed HFD for 25 weeks instead of 10 weeks similarly resulted in a lack of substantial weight gain or induction of signal switching (data

not shown). Thus, it remains unclear whether females are resistant to signal switching and weight gain and whether there is a causal relationship among these outcomes. Future studies using other obesogenic diets, and possibly genetic, surgical, or pharmacological models of obesity, will be required to disentangle the relationships among obesity, sex, G-protein signal switching, and integrative control of energy expenditure.

Finally, although data here indicate that activation/restoration of Gαi signaling in Type 1 AgRP neurons was sufficient to stimulate RMR regardless of diet, it remains unclear whether G-protein signal switching is a cause or consequence of excess weight gain. Future studies identifying the molecular mechanism of this signal switch are required, and studies purposefully inducing such signal switching will illuminate this issue. As highlighted here, one such mechanism that deserves exploration is the role of β-arrestin signaling within AgRP neurons. Pydi et al. previously implicated β-arrestin-1, but not β-arrestin-2, within AgRP neurons in energy balance and glycemic control.[30] In the present study, our data build upon these observations to more specifically implicate β-arrestin-1 in the transduction of AT_1R within the Type 1 subtype of AgRP neurons in lean animals, and hint that loss of β-arrestin-1 may contribute to signal switching by AT_1R in these cells. Thus, we hypothesize that mediators and modulators of G-protein signaling, such as β-arrestin-1, within AgRP neurons may contribute to the development of G-protein signal switching. Additional future studies to investigate the status and function of such mediators and modulators within individual subtypes of AgRP neurons during obesity and other pathological states are required.

STAR★METHODS

RESOURCE AVAILABILITY

Lead contact—Further information and requests for resources and reagents should be directed to the lead contact, Justin L. Grobe, PhD, (jgrobe@mcw.edu).

Materials availability—This study did not generate new unique reagents.

Data and code availability

- *Data*: All data reported in this paper will be shared by the lead contact upon request.
- *Code*: This paper does not report original code.
- Any additional information required to reanalyze the data reported in this paper is available from the lead contact upon request.

EXPERIMENTAL MODEL AND SUBJECT PARTICIPANT DETAILS

All animal procedures were approved by the Medical College of Wisconsin and University of Iowa Institutional Animal Care and Use Committees and were in accordance with the expectations laid out by the National Institutes of Health 8th guide for the care and use of laboratory animals. All mice were housed in ventilated cage racks at 22°C–24°C, with *ad libitum* access to food and filtered tap water unless otherwise noted. The following animal

models were used in this study: Male and female C57BL/6J mice were purchased from Jackson Laboratory (Jax 000664) at 6 weeks of age. *Agrp*-Cre[71] x Ai9[72] (Cre-dependent tdTomato reporter), in which tdTomato is expressed in all the cells that express AgRP.[9] P60 *Npy*-Gfp[73] mice (Jax 006417) that express GFP in all NPY expressing cells in ARC. BAC-*Agtr1a*-Cre x Ai9 mice that express Cre recombinase via the AT_{1A} locus[14] and their littermate controls were used in this study. To map whole-brain projections of Type 1i AT_{1A}-expressing AgRP/NPY neurons, we generated *Agtr1a*-Cre/*Npy*-FLP^+ mice by breeding BAC-*Agtr1a*-Cre females[14] to *Npy-Flp*[74] males. Briefly, all animals starting at 8 weeks of age were maintained in either standard chow (Teklad 2920x) or HFD (Research Diets D12451) for 10 weeks before use in experiments. Individual animal numbers used for each experiment are reported in the figure legend and/or within Table S1.

METHOD DETAILS

Drugs—The concentration of drugs was chosen from dose responses established in referenced previous studies. Compounds used were Angiotensin II (Ang-II, 2 mM,[75] Sigma, A9525), AT_1R antagonist losartan (LOS, 10 μM,[76] Sigma, 61188), AT_2R antagonist PD-123,319 (1 μM,[77] Sigma, P186), Gαi inhibitor Pertussis toxin (PTX, 500 ng/mL,[78] Sigma Aldrich; P7208), DREADD agonist, Clozapine N-oxide (CNO, 1 μM for electrophysiology, and 2 μg/g of body weight, i.p. for physiological measurements,[79] Tocris, 4936), GIRK/Kir3 inhibitor, Tertiapin Q (0.3 μM,[80] Tocris, 1316), VGCC agonist, FPL 64176 (4 μM,[81] Tocris, 1403), Voltage gated potassium channel (VGKC) inhibitor, 4 Aminopyridine (4-AP, 1 mM,[82] Tocris, 0940), Gαq inhibitor, BIM-46187 (10 μM,[83] Sigma, 5332990001), BK channel inhibitor, Penitrem A (0.5 mM,[84] Tocris, 4617), K^+/Cl^- co-transporter 2 (KCC2) inhibitor, VU 0463271 (10 mM,[85] Tocris, 4719), $Na^+/K^+/Cl^-$ co-transporter 1 (NKCC1) inhibitor, Bumetanide (10 μM,[86] Sigma, B3023), KCC2 agonist, CLP-257 (10 μM,[87] Tocris, 5242), VGCC inhibitor, Cilnidipine (5 μM,[88] Tocris, 2629), TRV027 (3 μM[89]), GeneScript). Stock solutions of Penitrem A (100 mM) were first dissolved in DMSO (Sigma-Aldrich) then diluted to a final concentration (0.03% DMSO) in aCSF for bath application (100 μM). All other drugs were dissolved in aCSF.

Food intake—Chow and HFD fed 18-week-old mice were singly housed in static home cages for assessing food intake. The first 24-h period was discarded for acclimation. Food intake, water intake, and feces output were all recorded.

Resting metabolic rate measurement/heat production—Resting metabolic rate was measured via respirometry as previously[90] described using Sable Systems FMS-3 gas analyzers. Mice were individually placed in an air-tight chamber maintained at thermoneutrality (30°C) and supplied with 400 mL/min air supply. Animals remain in the chamber until a clear plateau in VO_2 and VCO_2 were observed, which corresponds with the animal resting. STP-corrected rates of oxygen consumption and carbon dioxide production were determined from measures of VO_2, VCO_2, water vapor pressure, and mass flow of effluent air. Aerobic heat production was then estimated from measures of gas exchange using the modified Weir equation.[91] Analyzers were calibrated daily using a calibration gas mixture at 20.50% O_2 and 5000 ppm CO_2.

Stereotaxic injection of DREADDs in the arcuate nucleus—BAC-*Agtr1a*-Cre transgenic mice were bilaterally injected in the ARC (200 nL/side) with an Adeno-Associated Virus (AAV) encoding the Synapsin-1 promoter driving Cre-dependent expression of hM4Di or hM3Dq vector conjugated with a mCherry reporter (Addg- ene). The vectors were injected at a titer of 1.6×10^{13} GC/mL.[22] Each mouse was anesthetized with 2–3% isoflurane and placed in stereotaxic frame. Their skulls were exposed and leveled between lambda and bregma. A micromanipulator was oriented to lower the probe to the targeted coordinates of ARC (1.96 mm posterior, 5.80 mm ventral, and ±0.40 mm lateral from bregma). Each construct was injected in both the ARCs over a 10 min period. After 5 min, the injector was removed, and the incision was closed with sutures. The injection site was evaluated by light microscopy at the end of the study. Mice with injections located primarily in the ARC were included in the subsequent analyses. The specificity and the efficiency of the viral construct was verified by performing electrophysiological recordings.

Electrophysiology slice preparation—Mice were anesthetized with 2–3% isoflurane and decapitated. Hypothalamic slices containing the ARC were prepared similar to previously described approach.[76] Coronal slices (300 mm) containing the ARC were cut using a vibratome (Leica VT1200s) in ice-cold (0°C–1°C), oxygenated (95% O_2, 5% CO_2) cutting solution consisting of the following: 3 mM KCl, 1 mM $MgCl_2$-$6H_2O$, 2 mM $CaCl_2$, 2 mM $MgSO_4$, 1.25 mM NaH_2PO_4, 26 mM $NaHCO_3$, 10 mM D-glucose, and 206 mM sucrose (300 mOsm/kg H_2O, pH 7.4). Slices were incubated at room temperature (22°C) in oxygenated (95% O_2-5% CO_2) artificial cerebrospinal fluid (aCSF) containing 126 mM NaCl, 3 mM KCl, 2 mM $CaCl_2$, 2 mM $MgSO_4$, 1.25 mM NaH_2PO_4, 26 mM $NaHCO_3$, and 10 mM D-Glucose (300 mOsm/ kg H_2O, pH 7.4) for a minimum of 1 h before recording.

Slice preparation from P60 *Npy-Gfp* mice were performed using buffers with different compositions as detailed below and described previously.[92] Briefly, mice were sacrificed, and brains were immersed in NMDG-HEPES aCSF cutting solution (in mM): 92 NMDG, 2.5 KCl, 1.25 NaH_2PO_4, 30 $NaHCO_3$, 20 HEPES, 25 glucose, 2 thiourea, 5 Na-ascorbate, 3 Na-pyruvate, 0.5 $CaCl_2$·2H2O, and 10 $MgSO_4$·$7H_2O$. Brain tissue is kept in 95% O_2/5% CO_2 aerated ice-cold cutting solution and 300 μm thick fresh slices containing the hypothalamus were obtained with vibratome and transferred to 95% O_2/5% CO_2 aerated and HEPES containing artificial cerebrospinal fluid (aCSF) incubation solution containing (in mM): 92 NaCl, 2.5 KCl, 1.25 NaH_2PO_4, 30 $NaHCO_3$, 20 HEPES, 25 glucose, 2 thiourea, 5 Na-ascorbate, 3 Na-pyruvate, 2 $CaCl_2$·$2H_2O$, and 2 $MgSO_4$·7H2O. The sections were incubated in this solution for at least 30 min and placed in the recording chamber which has the recording aCSF (in mM): 124 NaCl, 2.5 KCl, 1.25 NaH_2PO_4, 24 $NaHCO_3$, 12.5 glucose, 5 HEPES, 2 $CaCl_2$·2 H_2O, and 2 $MgSO_4$·7 H_2O.

Loose cell recording—Slices containing the ARC were transferred to a submersion recording chamber and superfused with aCSF (31 ± 1°C, 1–2 mL/min). Slices were visualized using an upright fixed stage epifluorescent microscope (E600FN, Nikon) with differential interference contrast optics. GFP-expressing (in *Npy-Gfp* mice) or tdTomato-expressing (in *Agrp*-Cre x Ai9 or BAC-*Agtr1a*-Cre x Ai9 mice) AgRP neurons were

identified using epifluorescence and standard filters on the microscope equipped with a Cool Snap HQ^2 CCD camera (Photo- metrics, Inc).

Loose patch voltage clamp (extracellular) recordings were obtained using borosilicate glass micropipettes (1–3 MΩ) containing aCSF as the internal solution. Voltage was clamped at 0 mV to measure changes in current. Recordings were performed in the presence of the NMDA receptor antagonist D-2-amino-5-phosphonopentanoate (D-AP5; 50 μM), AMPA receptor antagonist 6-cyano-7-nitroquinoxaline-2,3-dione disodium salt (CNQX; 10 μM) and $GABA_A$ receptor antagonist picrotoxin (50 μM) unless otherwise stated. Recordings from ARC neurons were made by targeting GFP or tdTomato-expressing neurons in slices prepared from various transgenic mice. Baseline was first recorded for 5 min. The drugs were bath applied for 5 min (PTX 30 min) and were maintained throughout the following 5 min recording procedure. All recordings were performed at 32 ± 1°C using an automatic temperature controller (Warner Instruments). Electrophysiological signals (voltage and current) were amplified and digitized using MultiClamp 700B and Digidata 1440A, respectively using (Molecular Devices). Signals were filtered at 2 kHz and digitized at 10 kHz. Electrophysiological signals were obtained and analyzed using Axon pCLAMP 11.3 software. Spontaneous baseline firing rate of 2–5 min was monitored before administration of any drugs, neurons that remained within ±20% of baseline firing rate were classified as unaffected by the drug.

Whole cell recording—Whole cell recordings were performed in current clamp mode to measure membrane potential and firing rate of AgRP neurons in brain slices. Recordings were obtained using borosilicate glass micropipettes (3–8 MΩ). The internal pipette solution consisted of the following 145 mM K-gluconate, 10 mM HEPES, 1 mM EGTA, 2 mM Na_2ATP, and 0.4 mM NaGTP (300 mOsm/kg H_2O, pH 7.2). Recordings were made from ARC neurons with a series resistance of less than 25 MΩ following whole cell access. Neurons were slightly depolarized with current injection (current clamp) to generate a regular spiking activity (range, 50 to 40 mV), as previously described.[93,94] Liquid junction potential was corrected for within whole cell patch-clamp recordings automatically using the pipette offset on the patch-clamp amplifier and again calculated after recording. Parameters measured for action potential firing was spike count separated into 30 s bins.

GCaMP7 calcium imaging—P60 *Npy-gfp* mice were anesthetized with isoflurane and ~300 nL of rAAV2-*syn*-FLEX-jGCaMP7 virus[70] was injected bilaterally to ARC using a pulled glass pipette (Drummond Scientific) with 50 μm tip diameter as described previously.[95] The virus was injected at the rate of 30 nL/min by a micromanipulator (Narishige), allowing 10 min time for each injection. At least 3 weeks were given for animal recovery and transgene expression before further experiments. Slices were prepared as described above and CNQX (10 μM) + AP5 (50 μM) + PTX (50 μM) cocktail was added to the recording aCSF solution. Images were obtained on Scientifica SliceScope pro3000 using Hamamatsu Orca Flash 4.0v3 camera at 3Hz. A baseline of 5–10 min was imaged using 470 nm stimulation (CooLED PE4000) and GFP filter set 525/50m (Chroma) before bath administration of Ang-II (2 μM). Images were first background subtracted and ΔF values were obtained by subtracting baseline (F_0) fluorescence, which was defined as the

minimal fluorescence value in 5 min moving window. The area under the $\Delta F/F_0$ curve was calculated using Axon pCLAMP software before and after administration of Ang-II.

Anterograde tracing of neurons—Adult (8–12 weeks) *Agtr1a*-Cre$^+$/*Npy*-Flp$^+$ mice received stereotaxic microinjection of an AAV expressing ChR2-eYFP in both a Cre- and Flp-dependent manner (AAV-nEF-Con/Fon-ChR2-EYFP; Addgene# 137139) directly into the ARC. Stereotaxic surgery was performed as previously reported.[64,96] Briefly, mice were anesthetized by intraperitoneal (IP) injection of ketamine/xylazine (100/10 mg/kg) and placed on a Kopf stereotaxic apparatus. Following standard disinfection procedure, ~1.0 cm incision was made to expose the skull and a small hole was drilled into the skull unilaterally at defined positions to target the ARC. Pulled glass micropipette filled with AAV was slowly inserted to reach the ARC and a small volume (200 nL) of injection was made by applying pulse pressure using Tritech pressure Microinjector (Tritech Research). After 10 min of waiting to ensure full penetration of AAV, the needle was slowly retracted, and the incision closed by wound clips. Mice were kept on a warming pad until awake before returning to their home cages. After 3 weeks of recovery following AAV microinjection, mice were transcardially perfused, and the brains were extracted and cut into 30 μm of sections and the processed for FIHC to visualize EYFP fibers as reported.[64] A total of 9 mice received microinjection and 3 successfully targeted cases were used to evaluate the projections of Type 1i AgRP neurons throughout the brain.

QUANTIFICATION AND STATISTICAL ANALYSIS

Statistical analyses of data were performed using GraphPad Prism 9.5.1 and SPSS v27. Data were analyzed by independent t test, one- or two-way ANOVA or generalized linear modeling as noted in individual figure legends, with $p < 0.05$ considered statistically significant. Šidák multiple comparison procedures were used when main effects reached significance, to explore pairwise comparisons among groups. Throughout, summary data are reported as mean ± SEM.

Supplementary Material

Refer to Web version on PubMed Central for supplementary material.

ACKNOWLEDGMENTS

The authors gratefully acknowledge the assistance of Kelsey K. Wackman, KoTing Lu, and Medical College of Wisconsin institutional core facilities including the Comprehensive Rodent Metabolic Phenotyping Core and Engineering Core. This work was supported by the NIH (HL134850, HL084207, DK133121, HL144807, HL122358, HL153274, GM133421), American Heart Association (18EIA33890055, 898067, 826132, 903246, 22PRE898004), American Physiological Society, the Medical College of Wisconsin Clinical & Translational Science Institute “Obesity” Initiative (UL1TR001436), and the Advancing a Healthier Wisconsin Endowment.

REFERENCES

1. Blundell JE, Caudwell P, Gibbons C, Hopkins M, Naslund E, King N, and Finlayson G (2012). Role of resting metabolic rate and energy expenditure in hunger and appetite control: a new formulation. Dis. Model. Mech. 5, 608–613. 10.1242/dmm.009837. [PubMed: 22915022]
2. Oliveira V, Kwitek AE, Sigmund CD, Morselli LL, and Grobe JL (2021). Recent advances in hypertension: intersection of metabolic and blood pressure regulatory circuits in the central nervous

system. Hypertension 77, 1061–1068. 10.1161/HYPERTENSIONAHA.120.14513. [PubMed: 33611936]

3. Fothergill E, Guo J, Howard L, Kerns JC, Knuth ND, Brychta R, Chen KY, Skarulis MC, Walter M, Walter PJ, and Hall KD (2016). Persistent metabolic adaptation 6 years after "The Biggest Loser" competition. Obesity 24, 1612–1619. 10.1002/oby.21538. [PubMed: 27136388]
4. Mark AL (2013). Selective leptin resistance revisited. Am. J. Physiol. Regul. Integr. Comp. Physiol. 305, R566–R581. 10.1152/ajpregu.00180.2013. [PubMed: 23883674]
5. Morselli LL, Claflin KE, Cui H, and Grobe JL (2018). Control of energy expenditure by AgRP neurons of the arcuate nucleus: neurocircuitry, signaling pathways, and angiotensin. Curr. Hypertens. Rep. 20, 25. 10.1007/s11906-018-0824-8. [PubMed: 29556733]
6. Greenfield JR (2011). Melanocortin signalling and the regulation of blood pressure in human obesity. J. Neuroendocrinol. 23, 186–193. 10.1111/j.1365-2826.2010.02088.x. [PubMed: 21062377]
7. Grundlingh J, Dargan PI, El-Zanfaly M, and Wood DM (2011). 2,4-dinitrophenol (DNP): a weight loss agent with significant acute toxicity and risk of death. J. Med. Toxicol. 7, 205–212. 10.1007/s13181-011-0162-6. [PubMed: 21739343]
8. Goldgof M, Xiao C, Chanturiya T, Jou W, Gavrilova O, and Reitman ML (2014). The chemical uncoupler 2,4-dinitrophenol (DNP) protects against diet-induced obesity and improves energy homeostasis in mice at thermoneutrality. J. Biol. Chem. 289, 19341–19350. 10.1074/jbc.M114.568204. [PubMed: 24872412]
9. Claflin KE, Sandgren JA, Lambertz AM, Weidemann BJ, Littlejohn NK, Burnett CML, Pearson NA, Morgan DA, Gibson-Corley KN, Rahmouni K, and Grobe JL (2017). Angiotensin AT1A receptors on leptin receptor-expressing cells control resting metabolism. J. Clin. Invest. 127, 1414–1424. 10.1172/JCI88641. [PubMed: 28263184]
10. Sapouckey SA, Deng G, Sigmund CD, and Grobe JL (2017). Potential mechanisms of hypothalamic renin-angiotensin system activation by leptin and DOCA-salt for the control of resting metabolism. Physiol. Genom. 49, 722–732. 10.1152/physiolgenomics.00087.2017.
11. Wagner VA, Deng G, Claflin KE, Ritter ML, Cui H, Nakagawa P, Sigmund CD, Morselli LL, Grobe JL, and Kwitek AE (2023). Cell-specific transcriptome changes in the hypothalamic arcuate nucleus in a mouse deoxycorticosterone acetate-salt model of hypertension. Front. Cell. Neurosci. 17, 1207350. 10.3389/fncel.2023.1207350. [PubMed: 37293629]
12. Hilzendeger AM, Morgan DA, Brooks L, Dellsperger D, Liu X, Grobe JL, Rahmouni K, Sigmund CD, and Mark AL (2012). A brain leptin-renin angiotensin system interaction in the regulation of sympathetic nerve activity. Am. J. Physiol. Heart Circ. Physiol. 303, H197–H206. 10.1152/ajpheart.00974.2011. [PubMed: 22610169]
13. Deng G, Morselli LL, Wagner VA, Balapattabi K, Sapouckey SA, Knudtson KL, Rahmouni K, Cui H, Sigmund CD, Kwitek AE, and Grobe JL (2020). Single-nucleus RNA sequencing of the hypothalamic arcuate nucleus of C57BL/6J mice after prolonged diet-induced obesity. Hypertension 76, 589–597. 10.1161/HYPERTENSIONAHA.120.15137. [PubMed: 32507042]
14. Ritter ML, Deng G, Reho JJ, Deng Y, Sapouckey SA, Opichka MA, Balapattabi K, Wackman KK, Brozoski DT, Lu KT, et al. (2022). Cardiometabolic consequences of deleting the regulator of G protein signaling-2 (Rgs2) from cells expressing agouti-related peptide or the ANG (Angiotensin) II type 1A receptor in mice. Hypertension 79, 2843–2853. 10.1161/HYPERTENSIONAHA.122.20169. [PubMed: 36259376]
15. Lima LB, Pedroso JAB, Metzger M, Gautron L, and Donato J Jr. (2019). Relationship of alpha-MSH and AgRP axons to the perikarya of melanocortin-4 receptor neurons. Brain Res. 1717, 136–146. 10.1016/j.brainres.2019.04.021. [PubMed: 31009611]
16. Fenno LE, Ramakrishnan C, Kim YS, Evans KE, Lo M, Vesuna S, Inoue M, Cheung KYM, Yuen E, Pichamoorthy N, et al. (2020). Comprehensive dual- and triple-feature intersectional single-vector delivery of diverse functional payloads to cells of behaving mammals. Neuron 107, 836–853.e11. 10.1016/j.neuron.2020.06.003. [PubMed: 32574559]
17. Bagnol D, Lu XY, Kaelin CB, Day HE, Ollmann M, Gantz I, Akil H, Barsh GS, and Watson SJ (1999). Anatomy of an endogenous antagonist: relationship between Agouti-related protein and proopiomelanocortin in brain. J. Neurosci. 19, RC26. 10.1523/JNEUROSCI.19-18-j0004.1999. [PubMed: 10479719]

18. Wang D, He X, Zhao Z, Feng Q, Lin R, Sun Y, Ding T, Xu F, Luo M, and Zhan C (2015). Whole-brain mapping of the direct inputs and axonal projections of POMC and AgRP neurons. Front. Neuroanat. 9, 40. 10.3389/fnana.2015.00040. [PubMed: 25870542]
19. Yang Y, Smith DL Jr., Keating KD, Allison DB, and Nagy TR (2014). Variations in body weight, food intake and body composition after long-term high-fat diet feeding in C57BL/6J mice. Obesity 22, 2147–2155. 10.1002/oby.20811. [PubMed: 24942674]
20. Rahmouni K, Morgan DA, Morgan GM, Mark AL, and Haynes WG (2005). Role of selective leptin resistance in diet-induced obesity hypertension. Diabetes 54, 2012–2018. 10.2337/diabetes.54.7.2012. [PubMed: 15983201]
21. Collins S, Martin TL, Surwit RS, and Robidoux J (2004). Genetic vulnerability to diet-induced obesity in the C57BL/6J mouse: physiological and molecular characteristics. Physiol. Behav. 81, 243–248. 10.1016/j.physbeh.2004.02.006. [PubMed: 15159170]
22. Krashes MJ, Koda S, Ye C, Rogan SC, Adams AC, Cusher DS, Maratos-Flier E, Roth BL, and Lowell BB (2011). Rapid, reversible activation of AgRP neurons drives feeding behavior in mice. J. Clin. Invest. 121, 1424–1428. 10.1172/JCI46229. [PubMed: 21364278]
23. Liggett SB (2011). Phosphorylation barcoding as a mechanism of directing GPCR signaling. Sci. Signal. 4, pe36. 10.1126/scisignal.2002331. [PubMed: 21868354]
24. Gurevich VV, and Gurevich EV (2019). GPCR signaling regulation: the role of GRKs and arrestins. Front. Pharmacol. 10, 125. 10.3389/fphar.2019.00125. [PubMed: 30837883]
25. Haider RS, Matthees ESF, Drube J, Reichel M, Zabel U, Inoue A, Chevigné A, Krasel C, Deupi X, and Hoffmann C (2022). beta-arrestin1 and 2 exhibit distinct phosphorylation-dependent conformations when coupling to the same GPCR in living cells. Nat. Commun. 13, 5638. 10.1038/s41467-022-33307-8. [PubMed: 36163356]
26. Drube J, Haider RS, Matthees ESF, Reichel M, Zeiner J, Fritz-wanker S, Ziegler C, Barz S, Klement L, Filor J, et al. (2022). GPCR kinase knockout cells reveal the impact of individual GRKs on arrestin binding and GPCR regulation. Nat. Commun. 13, 540. 10.1038/s41467-022-28152-8. [PubMed: 35087057]
27. Matthees ESF, Haider RS, Hoffmann C, and Drube J (2021). Differential regulation of GPCRs-are GRK expression levels the key? Front. Cell Dev. Biol. 9, 687489. 10.3389/fcell.2021.687489. [PubMed: 34109182]
28. Lymperopoulos A, Borges JI, Carbone AM, Cora N, and Sizova A (2021). Cardiovascular angiotensin II type 1 receptor biased signaling: Focus on non-Gq-non-betaarrestin-dependent signaling. Pharmacol. Res. 174, 105943. 10.1016/j.phrs.2021.105943. [PubMed: 34662735]
29. Zhuang LN, Hu WX, Zhang ML, Xin SM, Jia WP, Zhao J, and Pei G (2011). Beta-arrestin-1 protein represses diet-induced obesity. J. Biol. Chem. 286, 28396–28402. 10.1074/jbc.M111.223206. [PubMed: 21543334]
30. Pydi SP, Cui Z, He Z, Barella LF, Pham J, Cui Y, Oberlin DJ, Egritag HE, Urs N, Gavrilova O, et al. (2020). Beneficial metabolic role of beta-arrestin-1 expressed by AgRP neurons. Sci. Adv. 6, eaaz1341. 10.1126/sciadv.aaz1341. [PubMed: 32537493]
31. Namkung Y, LeGouill C, Kumar S, Cao Y, Teixeira LB, Lukasheva V, Giubilaro J, Simões SC, Longpré JM, Devost D, et al. (2018). Functional selectivity profiling of the angiotensin II type 1 receptor using pathway-wide BRET signaling sensors. Sci. Signal. 11, eaat1631. 10.1126/scisignal.aat1631. [PubMed: 30514808]
32. Campbell JN, Macosko EZ, Fenselau H, Pers TH, Lyubetskaya A, Tenen D, Goldman M, Verstegen AMJ, Resch JM, McCarroll SA, et al. (2017). A molecular census of arcuate hypothalamus and median eminence cell types. Nat. Neurosci. 20, 484–496. 10.1038/nn.4495. [PubMed: 28166221]
33. Romanov RA, Zeisel A, Bakker J, Girach F, Hellysaz A, Tomer R, Alpár A, Mulder J, Clotman F, Keimpema E, et al. (2017). Molecular interrogation of hypothalamic organization reveals distinct dopamine neuronal subtypes. Nat. Neurosci. 20, 176–188. 10.1038/nn.4462. [PubMed: 27991900]
34. Shirai H, Takahashi K, Katada T, and Inagami T (1995). Mapping of G protein coupling sites of the angiotensin II type 1 receptor. Hypertension 25, 726–730. 10.1161/01.hyp.25.4.726. [PubMed: 7721423]

35. Wisler JW, Xiao K, Thomsen ARB, and Lefkowitz RJ (2014). Recent developments in biased agonism. Curr. Opin. Cell Biol. 27, 18–24. 10.1016/j.ceb.2013.10.008. [PubMed: 24680426]
36. Wingler LM, Skiba MA, McMahon C, Staus DP, Kleinhenz ALW, Suomivuori CM, Latorraca NR, Dror RO, Lefkowitz RJ, and Kruse AC (2020). Angiotensin and biased analogs induce structurally distinct active conformations within a GPCR. Science 367, 888–892. 10.1126/science.aay9813. [PubMed: 32079768]
37. Wingler LM, Elgeti M, Hilger D, Latorraca NR, Lerch MT, Staus DP, Dror RO, Kobilka BK, Hubbell WL, and Lefkowitz RJ (2019). Angiotensin analogs with divergent bias stabilize distinct receptor conformations. Cell 176, 468–478.e11. 10.1016/j.cell.2018.12.005. [PubMed: 30639099]
38. Fu Y, Huang Y, Yang Z, Chen Y, Zheng J, Mao C, Li Z, Liu Z, Yu B, Li T, et al. (2021). Cartilage oligomeric matrix protein is an endogenous beta-arrestin-2-selective allosteric modulator of AT1 receptor counteracting vascular injury. Cell Res. 31, 773–790. 10.1038/s41422-020-00464-8. [PubMed: 33510386]
39. Strachan RT, Sun JP, Rominger DH, Violin JD, Ahn S, Rojas Bie Thomsen A, Zhu X, Kleist A, Costa T, and Lefkowitz RJ (2014). Divergent transducer-specific molecular efficacies generate biased agonism at a G protein-coupled receptor (GPCR). J. Biol. Chem. 289, 14211–14224. 10.1074/jbc.M114.548131. [PubMed: 24668815]
40. Suomivuori CM, Latorraca NR, Wingler LM, Eismann S, King MC, Kleinhenz ALW, Skiba MA, Staus DP, Kruse AC, Lefkowitz RJ, and Dror RO (2020). Molecular mechanism of biased signaling in a prototypical G protein-coupled receptor. Science 367, 881–887. 10.1126/science.aaz0326. [PubMed: 32079767]
41. Liu CH, Gong Z, Liang ZL, Liu ZX, Yang F, Sun YJ, Ma ML, Wang YJ, Ji CR, Wang YH, et al. (2017). Arrestin-biased AT1R agonism induces acute catecholamine secretion through TRPC3 coupling. Nat. Commun. 8, 14335. 10.1038/ncomms14335. [PubMed: 28181498]
42. de Gasparo M, Catt KJ, Inagami T, Wright JW, and Unger T (2000). International union of pharmacology. XXIII. The angiotensin II receptors. Pharmacol. Rev. 52, 415–472. [PubMed: 10977869]
43. Forrester SJ, Booz GW, Sigmund CD, Coffman TM, Kawai T, Rizzo V, Scalia R, and Eguchi S (2018). Angiotensin II signal transduction: an update on mechanisms of physiology and pathophysiology. Physiol. Rev. 98, 1627–1738. 10.1152/physrev.00038.2017. [PubMed: 29873596]
44. Balakumar P, and Jagadeesh G (2014). A century old renin-angiotensin system still grows with endless possibilities: AT1 receptor signaling cascades in cardiovascular physiopathology. Cell. Signal. 26, 2147–2160. 10.1016/j.cellsig.2014.06.011. [PubMed: 25007996]
45. de Kloet AD, Pati D, Wang L, Hiller H, Sumners C, Frazier CJ, Seeley RJ, Herman JP, Woods SC, and Krause EG (2013). Angiotensin type 1a receptors in the paraventricular nucleus of the hypothalamus protect against diet-induced obesity. J. Neurosci. 33, 4825–4833. 10.1523/JNEUROSCI.3806-12.2013. [PubMed: 23486953]
46. Kawakami K, Yanagawa M, Hiratsuka S, Yoshida M, Ono Y, Hiroshima M, Ueda M, Aoki J, Sako Y, and Inoue A (2022). Heterotrimeric Gq proteins act as a switch for GRK5/6 selectivity underlying beta-arrestin transducer bias. Nat. Commun. 13, 487. 10.1038/s41467-022-28056-7. [PubMed: 35078997]
47. Nobles KN, Xiao K, Ahn S, Shukla AK, Lam CM, Rajagopal S, Strachan RT, Huang TY, Bressler EA, Hara MR, et al. (2011). Distinct phosphorylation sites on the β(2)-adrenergic receptor establish a barcode that encodes differential functions of β-arrestin. Sci. Signal. 4, ra51. 10.1126/scisignal.2001707. [PubMed: 21868357]
48. Gao J, Denys I, Shahien A, Sutphen J, and Kapusta DR (2020). Downregulation of brain Gα12 attenuates angiotensin II-dependent hypertension. Am. J. Hypertens. 33, 198–204. 10.1093/ajh/hpz176. [PubMed: 31677381]
49. Kapusta DR, Pascale CL, and Wainford RD (2012). Brain heterotrimeric $G\alpha i_2$-subunit protein-gated pathways mediate central sympathoinhibition to maintain fluid and electrolyte homeostasis during stress. FASEB J. 26, 2776–2787. 10.1096/fj.11-196550. [PubMed: 22459149]
50. Wainford RD, and Kapusta DR (2012). Functional selectivity of central Gα-subunit proteins in mediating the cardiovascular and renal excretory responses evoked by central α(2) -adrenoceptor activation in vivo. Br. J. Phar macol. 166, 210–220. 10.1111/j.1476-5381.2011.01662.x.

51. Wainford RD, Kurtz K, and Kapusta DR (2008). Central G-alpha subunit protein-mediated control of cardiovascular function, urine output, and vasopressin secretion in conscious Sprague-Dawley rats. Am. J. Physiol. Regul. Integr. Comp. Physiol. 295, R535–R542. 10.1152/ajpregu.00043.2008. [PubMed: 18525017]
52. Mogi M, Iwai M, and Horiuchi M (2007). Emerging concepts of regulation of angiotensin II receptors: new players and targets for traditional re- ceptors. Arterioscler. Thromb. Vasc. Biol. 27, 2532–2539. 10.1161/ATVBAHA.107.144154. [PubMed: 17717300]
53. Zou Y, Akazawa H, Qin Y, Sano M, Takano H, Minamino T, Makita N, Iwanaga K, Zhu W, Kudoh S, et al. (2004). Mechanical stress activates angiotensin II type 1 receptor without the involvement of angiotensin II. Nat. Cell Biol. 6, 499–506. 10.1038/ncb1137. [PubMed: 15146194]
54. Unal H, and Karnik SS (2014). Constitutive activity in the angiotensin II type 1 receptor: discovery and applications. Adv. Pharmacol. 70, 155–174. 10.1016/b978-0-12-417197-8.00006-7. [PubMed: 24931196]
55. Mouradian GC Jr., Liu P, Nakagawa P, Duffy E, Gomez Vargas J, Balapattabi K, Grobe JL, Sigmund CD, and Hodges MR (2022). Patch-to-seq and transcriptomic analyses yield molecular markers of functionally distinct brainstem serotonin neurons. Front. Synaptic Neurosci. 14, 910820. 10.3389/fnsyn.2022.910820. [PubMed: 35844900]
56. Wu Q, Howell MP, Cowley MA, and Palmiter RD (2008). Starvation after AgRP neuron ablation is independent of melanocortin signaling. Proc. Natl. Acad. Sci. USA 105, 2687–2692. 10.1073/pnas.0712062105. [PubMed: 18272480]
57. Egan OK, Inglis MA, and Anderson GM (2017). Leptin signaling in AgRP Neurons modulates puberty onset and adult fertility in mice. J. Neurosci. 37, 3875–3886. 10.1523/JNEUROSCI.3138-16.2017. [PubMed: 28275162]
58. Littlejohn NK, Keen HL, Weidemann BJ, Claflin KE, Tobin KV, Markan KR, Park S, Naber MC, Gourronc FA, Pearson NA, et al. (2016). Suppression of resting metabolism by the angiotensin AT2 receptor. Cell Rep. 16, 1548–1560. 10.1016/j.celrep.2016.07.003. [PubMed: 27477281]
59. Grobe JL, Grobe CL, Beltz TG, Westphal SG, Morgan DA, Xu D, de Lange WJ, Li H, Sakai K, Thedens DR, et al. (2010). The brain Renin-angiotensin system controls divergent efferent mechanisms to regulate fluid and energy balance. Cell Metab. 12, 431–442. 10.1016/j.cmet.2010.09.011. [PubMed: 21035755]
60. Oliveira V, Reho JJ, Balapattabi K, Ritter ML, Mathieu NM, Opichka MA, Lu KT, Grobe CC, Silva SD Jr., Wackman KK, et al. (2022). Chronic intracerebroventricular infusion of angiotensin II causes dose- and sex-dependent effects on intake behaviors and energy homeostasis in C57BL/6J mice. Am. J. Physiol. Regul. Integr. Comp. Physiol. 323, R410–R421. 10.1152/ajpregu.00091.2022. [PubMed: 35816717]
61. Grobe JL, Buehrer BA, Hilzendeger AM, Liu X, Davis DR, Xu D, and Sigmund CD (2011). Angiotensinergic signaling in the brain mediates metabolic effects of deoxycorticosterone (DOCA)-salt in C57 mice. Hypertension 57, 600–607. 10.1161/HYPERTENSIONAHA.110.165829. [PubMed: 21263123]
62. Oliveira V, Riedl RA, Claflin KE, Mathieu NM, Ritter ML, Balapattabi K, Wackman KK, Reho JJ, Brozoski DT, Morgan DA, et al. (2022). Melanocortin MC(4)R receptor is required for energy expenditure but not blood pressure effects of angiotensin II within the mouse brain. Physiol. Genom. 54, 196–205. 10.1152/physiolgenomics.00015.2022.
63. Balthasar N, Dalgaard LT, Lee CE, Yu J, Funahashi H, Williams T, Ferreira M, Tang V, McGovern RA, Kenny CD, et al. (2005). Divergence of melanocortin pathways in the control of food intake and energy expenditure. Cell 123, 493–505. 10.1016/j.cell.2005.08.035. [PubMed: 16269339]
64. Singh U, Jiang J, Saito K, Toth BA, Dickey JE, Rodeghiero SR, Deng Y, Deng G, Xue B, Zhu Z, et al. (2022). Neuroanatomical organization and functional roles of PVN MC4R pathways in physiological and behavioral regulations. Mol. Metab. 55, 101401. 10.1016/j.molmet.2021.101401. [PubMed: 34823066]
65. Moffitt JR, Bambah-Mukku D, Eichhorn SW, Vaughn E, Shekhar K, Perez JD, Rubinstein ND, Hao J, Regev A, Dulac C, and Zhuang X (2018). Molecular, spatial, and functional single-cell profiling of the hypothalamic preoptic region. Science 362, eaau5324. 10.1126/science.aau5324. [PubMed: 30385464]

66. Monge-Roffarello B, Labbe SM, Lenglos C, Caron A, Lanfray D, Samson P, and Richard D (2014). The medial preoptic nucleus as a site of the thermogenic and metabolic actions of melanotan II in male rats. Am. J. Physiol. Regul. Integr. Comp. Physiol. 307, R158–R166. 10.1152/ajpregu.00059.2014. [PubMed: 24808495]

67. Nakamura K, Nakamura Y, and Kataoka N (2022). A hypothalamomedullary network for physiological responses to environmental stresses. Nat. Rev. Neurosci. 23, 35–52. 10.1038/s41583-021-00532-x. [PubMed: 34728833]

68. Chen SR, Chen H, Zhou JJ, Pradhan G, Sun Y, Pan HL, and Li DP (2017). Ghrelin receptors mediate ghrelin-induced excitation of agouti-related protein/neuropeptide Y but not pro-opiomelanocortin neurons. J. Neurochem. 142, 512–520. 10.1111/jnc.14080. [PubMed: 28547758]

69. Secher A, Jelsing J, Baquero AF, Hecksher-Sørensen J, Cowley MA, Dalbøge LS, Hansen G, Grove KL, Pyke C, Raun K, et al. (2014). The arcuate nucleus mediates GLP-1 receptor agonist liraglutide-dependent weight loss. J. Clin. Invest. 124, 4473–4488. 10.1172/JCI75276. [PubMed: 25202980]

70. Dana H, Sun Y, Mohar B, Hulse BK, Kerlin AM, Hasseman JP, Tsegaye G, Tsang A, Wong A, Patel R, et al. (2019). High-performance calcium sensors for imaging activity in neuronal populations and microcompartments. Nat. Methods 16, 649–657. 10.038/s41592-019-0435-6. [PubMed: 31209382]

71. Tong Q, Ye CP, Jones JE, Elmquist JK, and Lowell BB (2008). Synaptic release of GABA by AgRP neurons is required for normal regulation of energy balance. Nat. Neurosci. 11, 998–1000. 10.1038/nn.2167. [PubMed: 19160495]

72. Madisen L, Zwingman TA, Sunkin SM, Oh SW, Zariwala HA, Gu H, Ng LL, Palmiter RD, Hawrylycz MJ, Jones AR, et al. (2010). A robust and high-throughput Cre reporting and characterization system for the whole mouse brain. Nat. Neurosci. 13, 133–140. 10.1038/nn.2467. [PubMed: 20023653]

73. van den Pol AN, Yao Y, Fu LY, Foo K, Huang H, Coppari R, Lowell BB, and Broberger C (2009). Neuromedin B and gastrin-releasing peptide excite arcuate nucleus neuropeptide Y neurons in a novel transgenic mouse expressing strong Renilla green fluorescent protein in NPY neurons. J. Neurosci. 29, 4622–4639. 10.1523/jneurosci.3249-08.2009. [PubMed: 19357287]

74. Daigle TL, Madisen L, Hage TA, Valley MT, Knoblich U, Larsen RS, Takeno MM, Huang L, Gu H, Larsen R, et al. (2018). A suite of transgenic driver and reporter mouse lines with enhanced brain-cell-type targeting and functionality. Cell 174, 465–480.e22. 10.1016/j.cell.2018.06.035. [PubMed: 30007418]

75. Cato MJ, and Toney GM (2005). Angiotensin II excites paraventricular nucleus neurons that innervate the rostral ventrolateral medulla: an in vitro patch-clamp study in brain slices. J. Neurophysiol. 93, 403–413. 10.1152/jn.01055.2003. [PubMed: 15356186]

76. Farmer GE, Balapattabi K, Bachelor ME, Little JT, and Cunningham JT (2018). AT(1a) influences GABAA-mediated inhibition through regulation of KCC2 expression. Am. J. Physiol. Regul. Integr. Comp. Physiol. 315, R972–R982. 10.1152/ajpregu.00105.2018. [PubMed: 30156863]

77. Matsuura T, KumaGαi H, Onimaru H, Kawai A, Iigaya K, Onami T, Sakata K, Oshima N, Sugaya T, and Saruta T (2005). Electrophysiological properties of rostral ventrolateral medulla neurons in angiotensin II 1a receptor knockout mice. Hypertension 46, 349–354. 10.1161/01.HYP.0000173421.97463.ac. [PubMed: 15998710]

78. Hatton GI, and Yang QZ (2001). Ionotropic histamine receptors and H2 receptors modulate supraoptic oxytocin neuronal excitability and dye coupling. J. Neurosci. 21, 2974–2982. 10.1523/JNEURO-SCI.21-09-02974.2001. [PubMed: 11312281]

79. Alexander GM, Rogan SC, Abbas AI, Armbruster BN, Pei Y, Allen JA, Nonneman RJ, Hartmann J, Moy SS, Nicolelis MA, et al. (2009). Remote control of neuronal activity in transgenic mice expressing evolved G protein-coupled receptors. Neuron 63, 27–39. 10.1016/j.neuron.2009.06.014. [PubMed: 19607790]

80. Philippart F, and Khaliq ZM (2018). G(i/o) protein-coupled receptors in dopamine neurons inhibit the sodium leak channel NALCN. Elife 7, e40984. 10.7554/eLife.40984. [PubMed: 30556810]

81. Liu Y, Harding M, Pittman A, Dore J, Striessnig J, Rajadhyaksha A, and Chen X (2014). Cav1.2 and Cav1.3 L-type calcium channels regulate dopaminergic firing activity in the mouse ventral tegmental area. J. Neurophysiol. 112, 1119–1130. 10.1152/jn.00757.2013. [PubMed: 24848473]

82. Smith C, Kongsamut S, Wang H, Ji J, Kang J, and Rampe D (2009). In Vitro electrophysiological activity of nerispirdine, a novel 4-aminopyridine derivative. Clin. Exp. Pharmacol. Physiol. 36, 1104–1109. 10.1111/j.1440-1681.2009.05200.x. [PubMed: 19413590]
83. Dantsuji M, Nakamura S, Nakayama K, Mochizuki A, Park SK, Bae YC, Ozeki M, and Inoue T (2019). 5-HT(2A) receptor activation enhances NMDA receptor-mediated glutamate responses through Src kinase in the dendrites of rat jaw-closing motoneurons. J. Physiol. 597, 2565–2589. 10.1113/JP275440. [PubMed: 30919966]
84. Abrahao KP, Chancey JH, Chan CS, and Lovinger DM (2017). Ethanol-sensitive pacemaker neurons in the mouse external globus pallidus. Neuropsychopharmacology 42, 1070–1081. 10.1038/npp.2016.251. [PubMed: 27827370]
85. Sivakumaran S, Cardarelli RA, Maguire J, Kelley MR, Silayeva L, Morrow DH, Mukherjee J, Moore YE, Mather RJ, Duggan ME, et al. (2015). Selective inhibition of KCC2 leads to hyperexcitability and epileptiform discharges in hippocampal slices and in vivo. J. Neurosci. 35, 8291–8296. 10.1523/JNEUROSCI.5205-14.2015. [PubMed: 26019342]
86. Balapattabi K, Farmer GE, Knapp BA, Little JT, Bachelor M, Yuan JP, and Cunningham JT (2019). Effects of salt-loading on supraoptic vasopressin neurones assessed by ClopHensorN chloride imaging. J. Neuroendocrinol. 31, e12752. 10.1111/jne.12752. [PubMed: 31136029]
87. Caballero R, Gómez R, Moreno I, Nuñez L, González T, Arias C, Guizy M, Valenzuela C, Tamargo J, and Delpón E (2004). Interaction of angiotensin II with the angiotensin type 2 receptor inhibits the cardiac transient outward potassium current. Cardiovasc. Res. 62, 86–95. 10.1016/j.cardiores.2003.12.029. [PubMed: 15023555]
88. Murai Y, Uneyama H, Ishibashi H, Takahama K, and Akaike N (2000). Preferential inhibition of L- and N-type calcium channels in the rat hippocampal neurons by cilnidipine. Brain Res. 854, 6–10. 10.1016/s0006-8993(99)02295-7. [PubMed: 10784100]
89. Kashihara T, Kawagishi H, Nakada T, Numaga-Tomita T, Kadota S, Wolf EE, Du CK, Shiba Y, Morimoto S, and Yamada M (2020). beta-Arrestin-Biased AT(1) Agonist TRV027 causes a neonatal-specific sustained positive inotropic effect without increasing heart rate. JACC. Basic Transl. Sci. 5, 1057–1069. 10.1016/j.jacbts.2020.08.011. [PubMed: 33294739]
90. Reho JJ, Nakagawa P, Mouradian GC Jr., Grobe CC, Saravia FL, Burnett CML, Kwitek AE, Kirby JR, Segar JL, Hodges MR, et al. (2022). Methods for the comprehensive in vivo analysis of energy flux, fluid homeostasis, blood pressure, and ventilatory function in rodents. Front. Physiol. 13, 855054. 10.3389/fphys.2022.855054. [PubMed: 35283781]
91. Weir JB (1949). New methods for calculating metabolic rate with special reference to protein metabolism. J. Physiol. 109, 1–9. 10.1113/jphysiol.1949.sp004363. [PubMed: 15394301]
92. Ting JT, Lee BR, Chong P, Soler-Llavina G, Cobbs C, Koch C, Zeng H, and Lein E (2018). Preparation of acute brain slices using an optimized N-Methyl-D-glucamine Protective recovery method. J. Vis. Exp. 10.3791/53825.
93. Grob M, Drolet G, and Mouginot D (2004). Specific Na+ sensors are functionally expressed in a neuronal population of the median preoptic nucleus of the rat. J. Neurosci. 24, 3974–3984. 10.1523/JNEUROSCI.3720-03.2004. [PubMed: 15102913]
94. Marciante AB, Wang LA, Farmer GE, and Cunningham JT (2019). Selectively inhibiting the median preoptic nucleus attenuates angiotensin II and hyperosmotic-induced drinking behavior and vasopressin release in adult male rats. eNeuro 6, ENEURO.0473–18.2019. 10.1523/ENEURO.0473-18.2019.
95. Atasoy D, Betley JN, Su HH, and Sternson SM (2012). Deconstruction of a neural circuit for hunger. Nature 488, 172–177. 10.1038/nature11270. [PubMed: 22801496]
96. Deng Y, Dickey JE, Saito K, Deng G, Singh U, Jiang J, Toth BA, Zhu Z, Zingman LV, Resch JM, et al. (2022). Elucidating the role of Rgs2 expression in the PVN for metabolic homeostasis in mice. Mol. Metab. 66, 101622. 10.1016/j.molmet.2022.101622. [PubMed: 36307046]

Highlights

- Three AgRP neuron subtypes are dissociated via electrochemical responses to Ang-II
- The Type 1 AgRP neuron subtype in lean mice is inhibited via AT_{1A} and a Gαi cascade
- Obesity induces a spontaneous AT_{1A}-Gαi to -Gαq signal switch in Type 1 AgRP neurons
- The loss of AT_{1A}-Gαi coupling in Type 1 AgRP neurons contributes to RMR adaptation

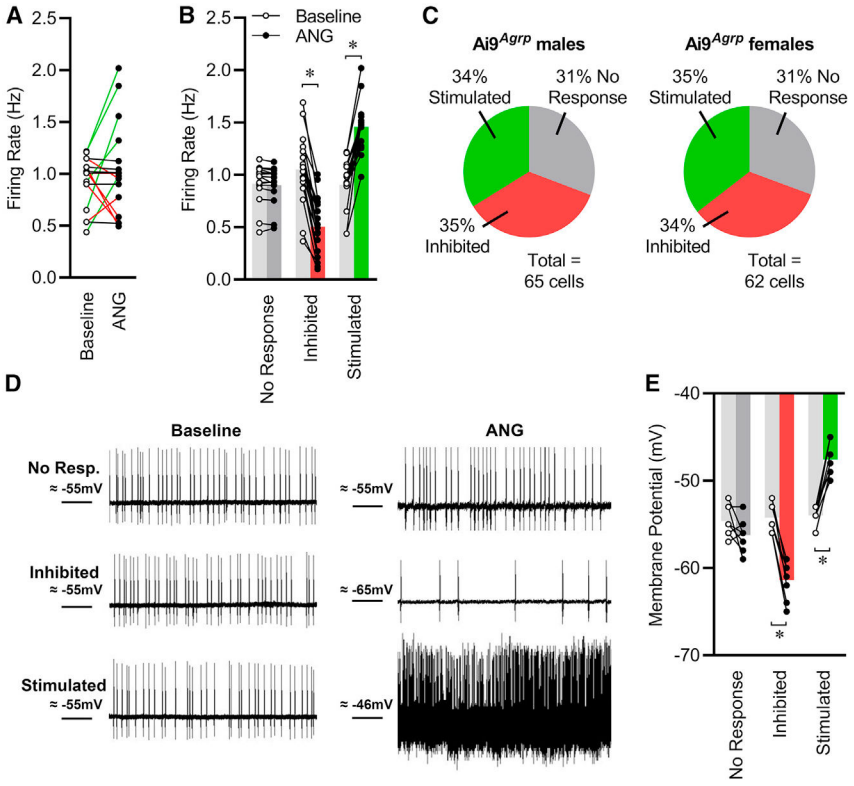

Figure 1. Ang-II causes distinct electrical responses in individual AgRP neurons of chow-fed mice

(A) Initial analyses of firing-rate responses of individual AgRP neurons to application of Ang-II (n = 18 cells).

(B) Cells were grouped into three subtypes according to electrical responses to Ang-II: no response, inhibited, or stimulated by Ang-II (n = 15–17 per response).

(C) Pie chart illustrating the relative distribution of AgRP neuron subtypes in chow-fed mice of each sex.

(D) Example tracings of three subtypes under baseline and Ang-II-stimulated conditions.

(E) Current clamping demonstrates a similar distribution of subtypes of AgRP neuron within the ARC (n = 7–8 per response).

*p < 0.05 by Šidák multiple comparisons procedure (A, B, E); summary data are presented as mean ± SEM. Replicates are indicated by individual dots or summaries within each panel. See also Figure S1.

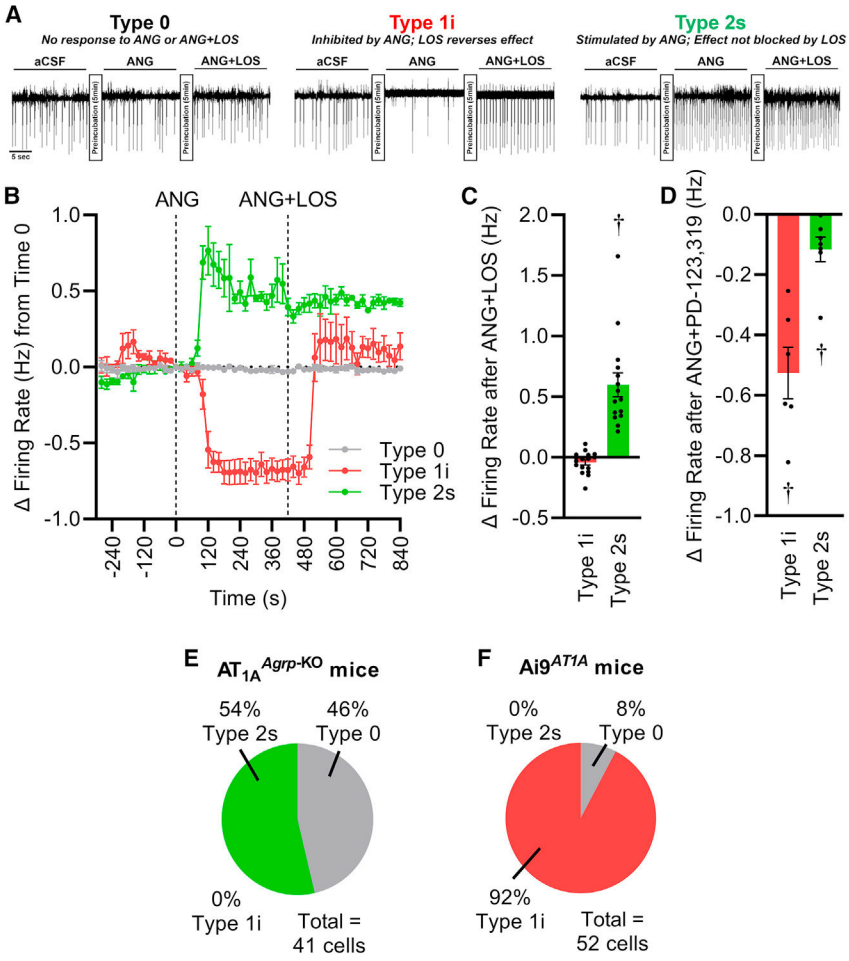

Figure 2. Ang-II inhibits Type 1i AgRP neurons via AT_1R, and stimulates Type 2s AgRP neurons via AT_2R

(A) Example tracings from Type 0, Type 1i, and Type 2s neurons after application of Ang-II, and subsequently Ang-II in the presence of the AT_1R antagonist losartan (LOS).

(B) Example quantification of changes in firing rate of Type 0, Type 1i, and Type 2s neurons (n = 4–5 each) in response to Ang-II versus Ang-II + LOS. Note the normalization of firing rate of Type 1i neurons by LOS, but the lack of effect of LOS in Type 2s neurons.

(C) Quantification of the firing rate of Type 1i and Type 2s neurons after Ang-II + LOS application, relative to baseline firing rates (n = 17, 15).

(D) Quantification of the firing rate of Type 1i and Type 2s neurons (n = 6, 7) after application of Ang-II in the presence of the AT_2R antagonist PD-123319, relative to baseline firing rates.

(E) Pie chart illustrating the relative abundance of Type 0 and Type 2s neurons, and the lack of Type 1i neurons, in mice with conditional genetic deletion of *Agtr1a* (AT_{1A} receptor) from all AgRP neurons ($AT_{1A}^{Agrp\text{-}KO}$ mice).

(F) Pie chart illustrating firing-rate responses of neurons within the ARC that express AT_{1A} ($Ai9^{AT1A}$ mice) to acute Ang-II application.

†$p < 0.05$ versus zero by one-sample t test (C and D); summary data are presented as mean ± SEM. Replicates are indicated by individual dots or summaries within each panel. See also Figure S2.

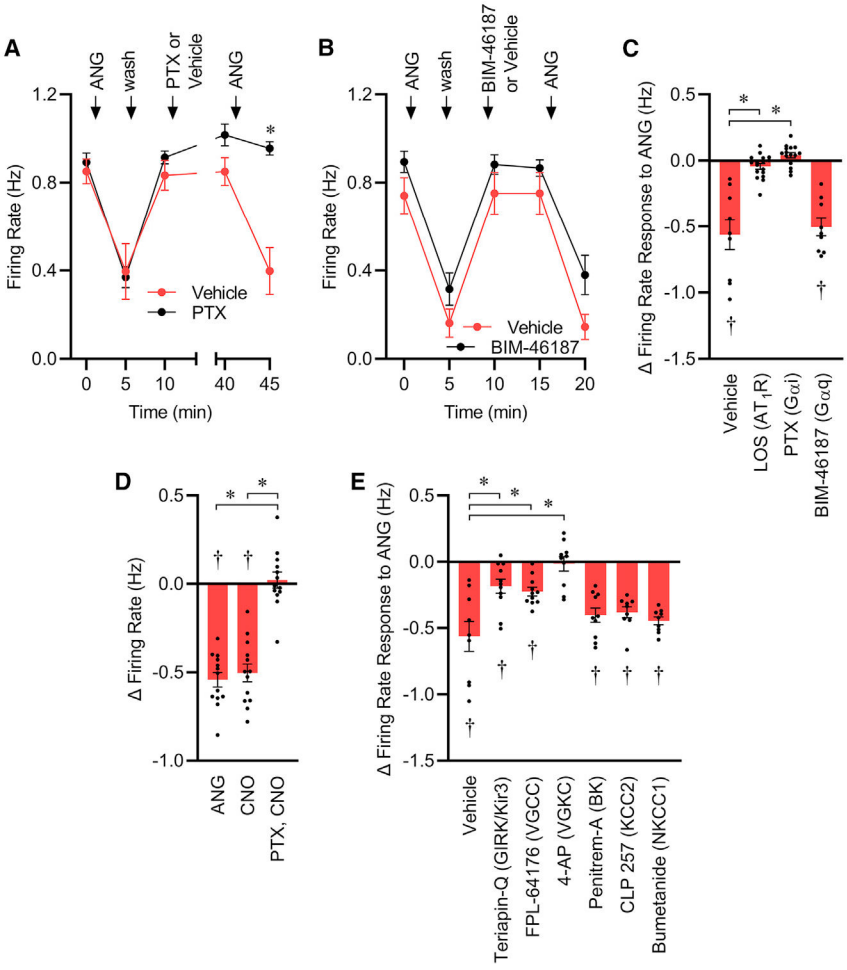

Figure 3. Ang-II inhibits Type 1i neurons through a cascade involving Gαi, inward-rectifier, and voltage-gated potassium channels, and L-type calcium channels

(A–C) Changes in firing rates of Type 1i neurons from the ARC of Ai9^{Agrp} mice in response to Ang-II after pharmacological blockade of Gαi via pertussis toxin (PTX), or Gαq via BIM-46187. (A) Time course of responses to Ang-II before and after incubation with vehicle (n = 6) or PTX (n = 15). (B) Time course of responses to Ang-II before and after application of vehicle (n = 6) or BIM-46187 (n = 9). (C) Quantification of responses after preincubation with vehicle (n = 9), losartan (LOS, n = 17), PTX (n = 15), or BIM (n = 9).

(D) Changes in firing rate of Type 1i neurons (identified by inhibitory response to Ang-II, n = 13) from the ARC of mice expressing the Gαi-coupled hM4Di DREADD in AgRP neurons (hM4Di^{Agrp} mice), in response to clozapine *N*-oxide (CNO) with or without pretreatment with PTX.

(E) Summary of responses of Type 1i neurons from the ARC of Ai9^{Agrp} mice in response to Ang-II after pretreatment with vehicle or selected channel inhibitors (n = 9–11 per inhibitor).

*$p < 0.05$ as indicated by Šidák multiple comparisons procedure, $^{\dagger}p < 0.05$ versus zero by one-sample t test; summary data are presented as mean ± SEM. Replicates are indicated by individual dots. See also Figure S3.

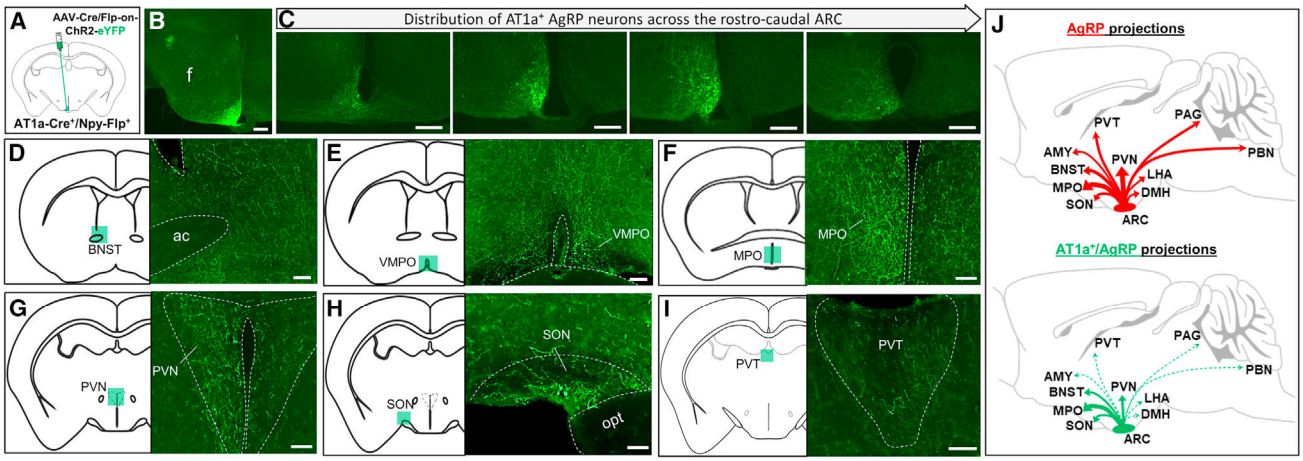

Figure 4. Type 1i neurons project to a subset of brain regions that are known to receive ARC AgRP inputs

(A) Schematic drawing of the strategy for unilateral anterograde tracing of AT_{1A}-expressing AgRP (Type 1i) neurons.

(B) Representative image showing the precise unilateral targeting of Type 1i AgRP neurons by ChR2-eYFP.

(C) Representative images showing the distribution of Type 1i AgRP neurons across the rostrocaudal ARC.

(D–I) Representative images showing the projections of ARC Type 1i neurons to (D) bed nucleus of the stria terminalis (BNST), (E) ventromedial preoptic nucleus (VMPO), (F) medial preoptic nucleus (MPO), (G) paraventricular nucleus of hypothalamus (PVN), (H) supraoptic nucleus (SON), and (I) paraventricular nucleus of the thalamus (PVT).

(J) Schematic diagram depicting the projections of ARC AgRP neurons (red) versus the Type 1i subtype (green). Additional structures: DMH, dorsomedial hypothalamic nucleus; LHA, lateral hypothalamic area; ARC, arcuate hypothalamic nucleus; AMY, amygdala; PBN, parabrachial nucleus; PAG, periaqueductal gray; ac, anterior commissure; f, fornix; opt, optic tract.

Scale bars represent 200 μm (B–G), 50 μm (H), and 100 μm (I). See also Figure S4.

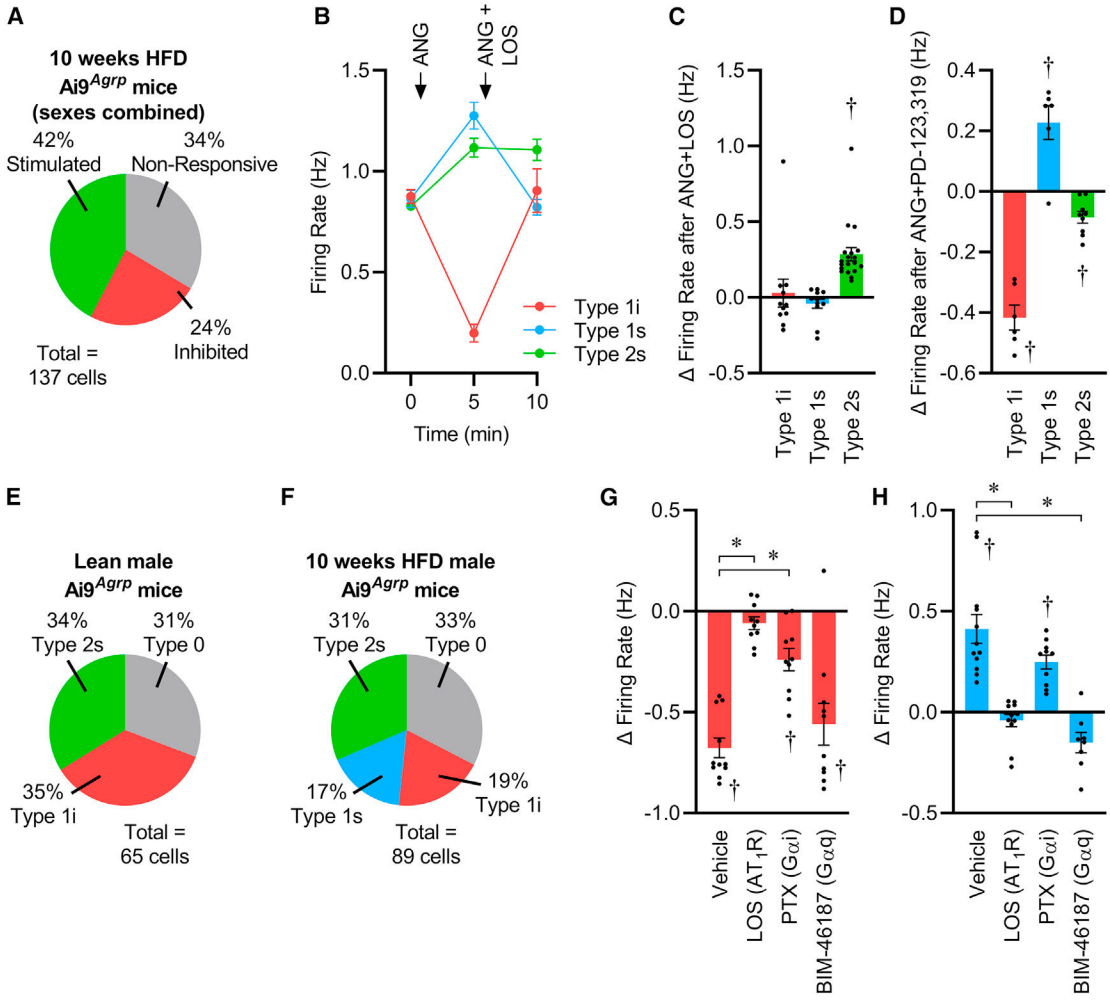

Figure 5. Ten weeks of high-fat diet (HFD; 45% kcal from fat) induces a G-protein signal switch within a subset of Type 1i AgRP neurons

(A) Ten weeks of HFD altered the relative proportion of AgRP neurons that were unaffected, inhibited, or stimulated by Ang-II in Ai9^{AgRP} mice (distribution $p < 0.05$ versus Figure 1C), with an increased representation of AgRP neurons that were stimulated by Ang-II.

(B) Time course of firing-rate responses of ARC AgRP neurons from HFD-fed Ai9^{Agrp} mice to acute application of Ang-II before and after AT_1R blockade by losartan (LOS). Notably, a subset of cells (Type 1s) are stimulated by Ang-II through a mechanism that is sensitive to blockade by LOS. Type 1i, n = 11; Type 1s, n = 12; Type 2s, n = 20.

(C and D) Summary of firing-rate responses of Type 1i, Type 1s, and Type 2s neurons to Ang-II after pretreatment with LOS (C; n = 11, 12, 20) or the AT_2R antagonist PD-123319 (D; n = 6, 6, 9).

(E) Pie chart summarizing the distribution of AgRP neuron subtypes in chow-fed male Ai9^{AgRP} mice.

(F) Pie chart summarizing the distribution of AgRP neuron subtypes in HFD-fed male Ai9^{AgRP} mice.

(G and H) Summary of firing-rate responses of Type 1i (G; n = 10–11 each) or Type 1s (H; n = 8–12 each) neurons (identified by LOS-dependent inhibition or stimulation, respectively)

to acute Ang-II application after pretreatment with the Gαi inhibitor, pertussis toxin (PTX) or the Gαq inhibitor, BIM-46187.

*$p < 0.05$ as indicated by Šidák multiple comparisons procedure, $^{\dagger}p < 0.05$ versus zero by one-sample t test (B, C, D, G, H); summary data are presented as mean ± SEM. Replicates are indicated by individual dots or summaries within each panel. See also Figure S5.

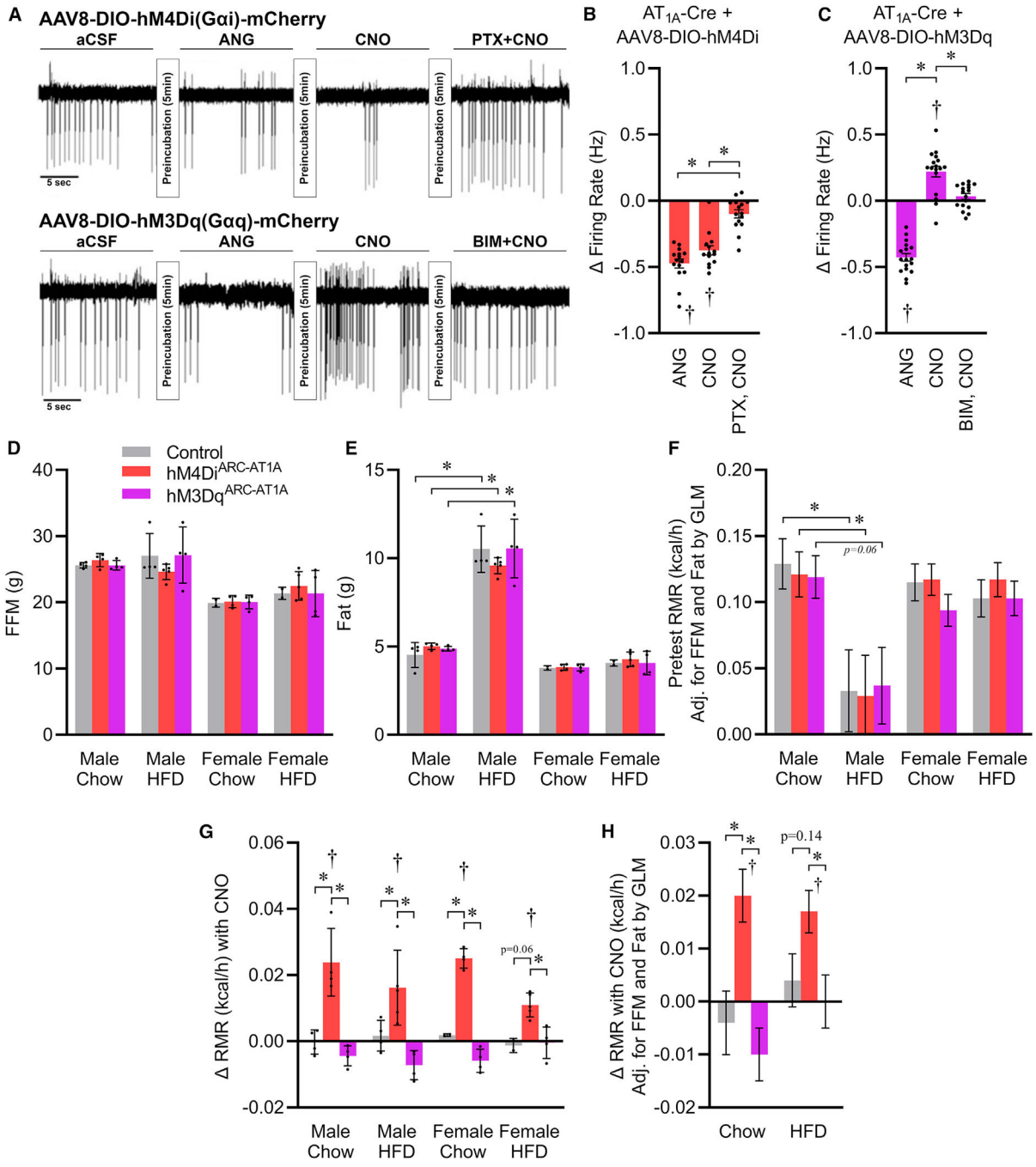

Figure 6. Activation of Gαi within Type 1 AgRP neurons is sufficient to stimulate RMR

(A) Example tracings from Ang-II-inhibited (Type 1i) AgRP neurons from hM4Di$^{ARC\text{-}AT1A}$ and hM3Dq$^{ARC\text{-}AT1A}$ mice, demonstrating pertussis toxin (PTX)-sensitive Gαi-mediated inhibition or BIM-46187 (BIM)-sensitive Gαq-mediated stimulation, respectively, in response to clozapine *N*-oxide (CNO).

(B and C) Quantification of effects of activating Gαi or Gαq within multiple Type 1i neurons from hM4Di$^{ARC\text{-}AT1A}$ (B; n = 15) and hM3Dq$^{ARC\text{-}AT1A}$ (C; n = 17) mice.

(D and E) Fat-free mass (FFM) (D) and fat mass (E) of mice after 10 weeks of chow or HFD feeding.

(F) RMR immediately preceding injection of CNO, corrected for body composition by GLM.

(G) Change in RMR with injection of CNO.

(H) Change in RMR with injection of CNO, with sexes combined, corrected for body composition by GLM.

For (D) to (G), control: n = 4 males + 2 females each diet; $hM4Di^{ARC\text{-}AT1A}$: n = 4 males + 4 females fed chow versus 5 males and 5 females fed HFD; $hM3Dq^{ARC\text{-}AT1A}$: n = 4 males + 4 females each diet.

For all panels except (A), $^{*}p < 0.05$ as indicated by Šidák multiple comparisons procedure, $^{\dagger}p < 0.05$ versus zero by one-sample t test; summary data are presented as mean ± SEM. Replicates are indicated by individual dots within each panel. See also Figure S6.

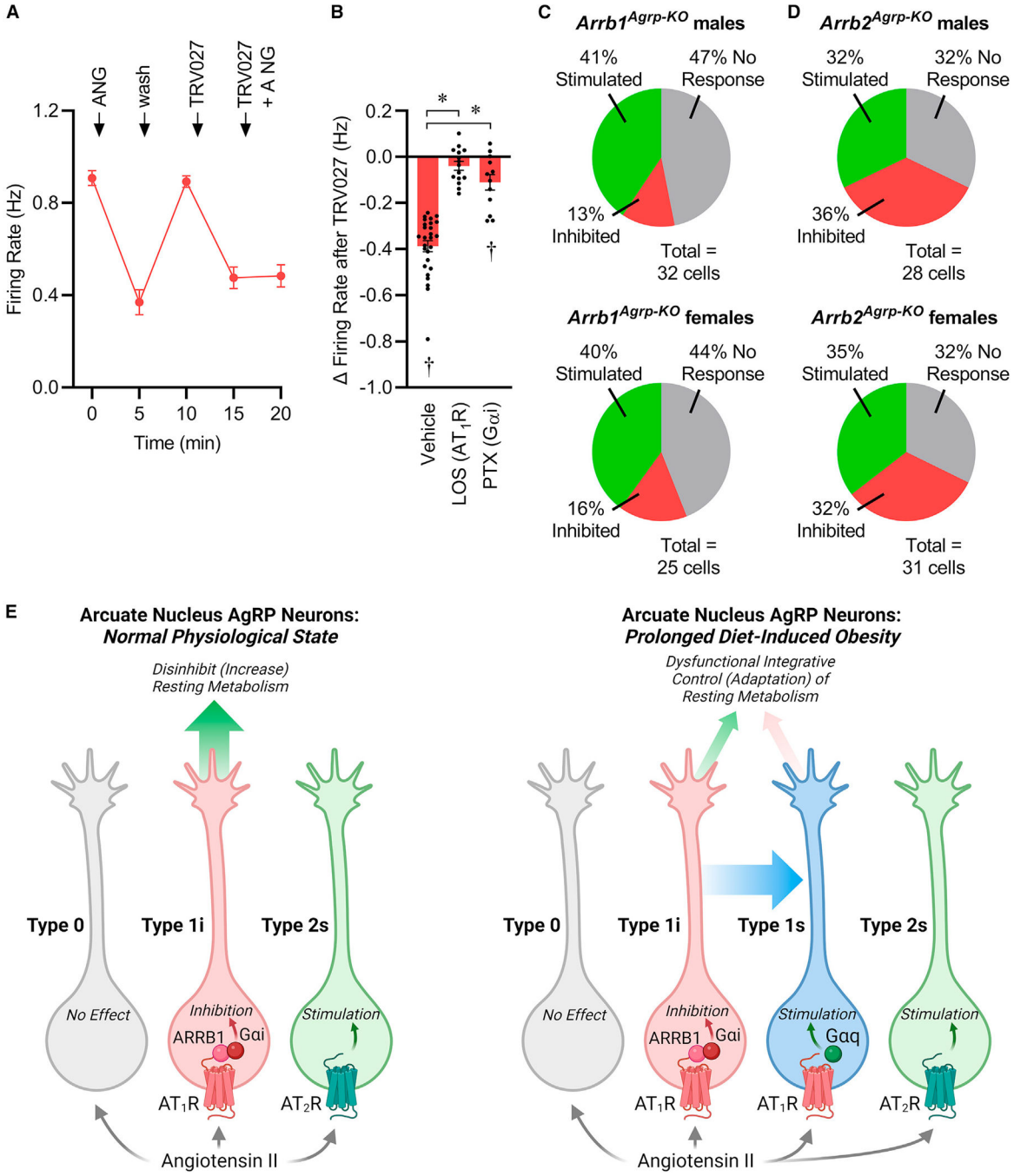

Figure 7. Implication of β-arrestin in AT_1R signaling within Type 1i neurons, and overall working model

(A) Firing rates of Type 1i neurons from the ARC of $Ai9^{Agrp}$ mice in response to Ang-II, TRV027, or TRV027 in the presence of Ang-II (n = 12). Summary data are presented as mean ± SEM.

(B) Quantification of change in firing rates of Type 1i neurons in response to TRV027 after preincubation with vehicle (n = 27), losartan (LOS, n = 15), or pertussis toxin (PTX, n = 12). *$p < 0.05$ as indicated by Šidák multiple comparisons procedure, †$p < 0.05$ versus zero by one-sample t test; summary data are presented as mean ± SEM

(C) Pie charts illustrating the relative distribution of ARC AgRP neuron responses to Ang-II in chow-fed *Arrb1*$^{Agrp\text{-KO}}$ mice.

(D) Pie charts illustrating the relative distribution of ARC AgRP neuron responses to Ang-II in chow-fed *Arrb2*$^{Agrp\text{-KO}}$ mice.

(E) Under normal physiological conditions, Ang-II acts on the Type 1i subtype of AgRP neuron within the ARC via its AT_1R and a second-messenger cascade involving both β-arrestin-1 and Gαi to cause inhibition of the cell. This results in reduced inhibitory neurotransmission to postsynaptic neurons, ultimately resulting in increased resting metabolism. Following prolonged obesity, a fraction of Type 1i AgRP neurons undergoes a spontaneous G-protein "signal switch," whereby AT_1R stops coupling via this cascade to inhibit the cell and instead begins coupling via the Gαq cascade to stimulate the cell. Resulting net increases in inhibitory neurotransmission to postsynaptic targets are expected to contribute to the pathological adaptation of resting metabolic rate control that is often observed with obesity.

KEY RESOURCES TABLE

REAGENT or RESOURCE	SOURCE	IDENTIFIER
Bacterial and virus strains		
pAAV-hSyn-DIO-hM4D(Gi)-mCherry (AAV8)	Krashes et al.[22]	Addgene 44362-AAV8
pAAV-hSyn-DIO-hM3D(Gq)-mCherry (AAV8)	Krashes et al.[22]	Addgene 44361-AAV8
AAV-nEF-Con/Fon-ChR2-EYFP	Fenno et al.[16]	Addgene 137139
rAAV2-syn-FLEX-]GCaMP7	Dana et al.[70]	N/A
Chemicals, peptides, and recombinant proteins		
Angiotensin II	Sigma	Cat# A9525
Losartan	Sigma	Cat# 61188
PD 123,319	Sigma	Cat# P186
Pertussis toxin (PTX)	Sigma Aldrich	Cat# P7208
Clozapine N-oxide (CNO)	Tocris	Cat# 4936
Tertiapin Q	Tocris	Cat# 1316
FPL 64176	Tocris	Cat# 1403
4 Aminopyridine (4-AP)	Tocris	Cat# 0940
BIM-46187	Sigma	Cat# 5332990001
Penitrem A	Tocris	Cat# 4617
VU 0463271	Tocris	Cat# 4719
Bumetanide	Sigma	Cat# B3023
CLP-257	Tocris	Cat# 5242
Cilnidipine	Tocris	Cat# 2629
TRV 120027 (TRV027)	GenSript	Custom synthesis (Sar^1-Arg^2-Val^3-Tyr^4-Ile^5- His^6-Pro^7-D-Ala^8-OH)
Experimental models: Organisms/strains		
C57BL/6J		Jackson Labs 000664
Agrp-Cre	Tong et al.[71]	Jackson Labs 012899
Ai9	Madison et al.[72]	Jackson Labs 007909
Npy-GFP	van den Pol et al.[73]	Jackson Labs 006417
BAC-AT1A-Cre	Ritter et al.[14]	N/A
Npy-FLP	Daigle et al.[74]	Jackson Labs 030211
Software and algorithms		
ImageJ		https://imagej.nih.gov/ij/
Graphpad Prism		https://www.graphpad.com/
SPSS Statistics		https://www.ibm.com/products/spss-statistics